Quantification of multiple simultaneously occurring nitrogen flows in the euphotic ocean

Min Nina Xu[1], Yanhua Wu[2], Li Wei Zheng[1], Zhenzhen Zheng[1], Huade Zhao[3], Edward A Laws[4], Shuh-Ji Kao[1]*

[1]State Key Laboratory of Marine Environmental Science, Xiamen University, Xiamen, China

[2]Shenzhen Marine Environment Monitoring Center Station, Shenzhen, China

[3]National Marine Environmental Monitoring Center, Dalian, China

[4]Environmental Sciences Department, School of the Coast & Environment, Louisiana State University, USA

Correspondence to: Shuh-Ji Kao (sjkao@xmu.edu.cn)

Abstract

The general features of the N cycle in the sunlit region of the ocean are well known, but methodological difficulties have previously confounded simultaneous quantification of transformation rates among the many different forms of N, e.g., ammonium (NH_4^+), nitrite (NO_2^-), nitrate (NO_3^-), and particulate/dissolved organic nitrogen (PN/DON). However, recent advances in analytical methodology have made it possible to employ a convenient isotope labeling technique to quantify *in situ* fluxes among oft-measured nitrogen species within the euphotic zone. Addition of a single ^{15}N-labeled NH_4^+ tracer and monitoring of the changes in the concentrations and isotopic compositions of the total dissolved nitrogen (TDN), PN, NH_4^+, NO_2^-, and NO_3^- pools allowed us to quantify the ^{15}N and ^{14}N fluxes simultaneously. Constraints expressing the balance of ^{15}N and ^{14}N fluxes between the different N pools were expressed in the form of simultaneous equations, the unique solution of which via matrix inversion yielded the relevant N fluxes, including rates of NH_4^+, NO_2^-, and NO_3^- uptake; ammonia oxidation; nitrite oxidation; DON release, and NH_4^+ uptake by bacteria. The matrix inversion methodology that we used was designed specifically to analyze the results of incubations under simulated *in situ* conditions in the euphotic zone. By taking into consideration simultaneous fluxes among multiple N pools, we minimized potential artifacts caused by non−targeted processes in traditional source-product methods. The proposed isotope matrix method facilitates post-hoc analysis of data from on-deck incubation experiments and can be used to probe effects

of environmental factors (e.g., pH, temperature, and light) on multiple processes under controlled conditions.

Keywords

Ammonium oxidation, isotope, new production, nitrification, regenerated production

1. Introduction

Nitrogen (N), which is an essential element for all organisms, regulates productivity in the surface waters of many parts of the ocean (Falkowski, 1997; Zehr and Kudela, 2011; Casciotti, 2016). As a limiting nutrient in the euphotic zone, nitrogen rapidly interconverts among five major N compartments: particulate organic nitrogen (PN), dissolved organic nitrogen (DON), ammonium (NH_4^+), nitrite (NO_2^-), and nitrate (NO_3^-) (Fig. 1). Studies of the rates of transformation of N in the marine N-cycle have had a major impact on our current understanding of the coupling of autotrophic and heterotrophic processes involving carbon and nitrogen as well as the efficiency of the biological pump (Dugdale and Goering, 1967; Caperon et al., 1979; Harrison et al., 1992; Bronk and Glibert, 1994; Dore and Karl, 1996; Laws et al., 2000; Yool et al., 2007). Such information has also facilitated evaluation of ecosystem functions. However, those studies have typically involved inventory and isotope tracer methods that quantified the rates of only one or a few fluxes (Ward, 2008, 2011; Lipschultz, 2008 and references therein). The dynamic nature and complexity of the N cycle make simultaneous resolution of the rates of more than a few of the important fluxes a challenging task.

The inventory method (monitoring the change of substrate and/or product concentrations over time) has often been used to determine the uptake rates of ammonium, nitrite, nitrate, and urea (McCarthy and Eppley, 1972; Harvey and Caperon, 1976; Harrison and Davis, 1977; Howard et al., 2007) and to examine the occurrence

and rate of nitrification (Wada and Hatton, 1971; Pakulski et al., 1995; Ward, 2011). However, failure to account for other processes may bias the results. For example, the concentration of ammonium is controlled simultaneously by removal via phytoplankton uptake (PN as the product), nitrification (nitrite/nitrate as the product), and bacterial metabolism (operationally defined DON as product) and by additions via remineralization from heterotrophic bacterial metabolism, zooplankton excretion, and viral lysis. Similarly, the products of nitrification (NO_x^-) may be simultaneously consumed by phytoplankton.

The ^{15}N-labeled tracer technique has been widely used as an assay for specific nitrogen processes since the emergence of isotope ratio mass spectrometry (IRMS). For example, the addition of ^{15}N-labeled nitrate has been applied to estimate new production (Dugdale and Goering, 1967; Chen, 2005; Painter et al., 2014). Likewise, by incubating water to which $^{15}NH_4^+$ has been added, the nitrification rate ($^{15}NO_3^-$ as product; e.g. Newell et al., 2013; Hsiao et al., 2014; Peng et al., 2016) and ammonium uptake rate ($^{15}N_{PN}$ as product; e.g. Dugdale and Goering, 1967; Dugdale and Wilkerson, 1986; Bronk et al., 1994, 2014) can be measured via incubations in the dark and light, respectively. However, the interpretation of isotope labeling experiments is confounded by the same problems as the inventory method, i.e., multiple processes that occur simultaneously impact the concentrations of substrates and products in the incubation bottle. In fact, those transformations among pools have significant implications for biogeochemical cycles. For instance, Yool et al. (2007) has

synthesized available global data and concluded that the fractional contribution of nitrate derived from nitrification to nitrate uptake can be as high as 19–33% in the euphotic zone. However, integration of the relevant rates over a light:dark cycle has been confounded by the fact that nitrate uptake rates have typically been determined during the photoperiod, whereas nitrification rates have been measured under dark conditions (e.g. Grundle et al., 2013). Nitrate uptake may occur in the dark, but not necessarily at the same rate as in the light (Laws and Wong, 1978), and nitrification is inhibited by light (Dore and Karl, 1996). To integrate rates over the light:dark cycle, 24-h incubations have been used to compensate for the diel cycle of light-sensitive processes (Beman et al., 2012). Yet, interpretation of the results of 24-h incubations may be confounded by artifacts due to transfers of ^{15}N and ^{14}N among pools. A new method is needed to overcome these problems.

Marchant et al. (2016) have reviewed recent methodological advances using ^{15}N-labeling substrates combined with nanoSIMS, FISH, or HISH in marine N-cycle studies. These methods provide qualitative information about N transfers at the cellular and molecular level but do not quantify rates at the community level. Elskens et al. (2005) conducted a comprehensive review of oft-used models for rate derivation and concluded that oversimplified models may lead to biased results if their underlying assumptions are violated. However, overly complex models risk misinterpreting random noise as relevant processes. To address this concern, De Brauwere et al. (2005) proposed a model selection procedure. More recently, Pfister et al. (2016) have applied

an isotope tracer technique and mass conservation model to explore nitrogen flows among dissolved nitrogen pools (NH_4^+, NO_2^-, and NO_3^-) in tidal pools and found that benthic macrobiota played an important role in regulating remineralization rates. They also found that dilution effects significantly biased the results obtained with source-product models. For the euphotic zone, where competing processes co-occur, an innovative and convenient method is needed to determine the rates of multiple N fluxes from the results of simulated *in-situ* incubations.

In this study, we propose an "isotope matrix method". To avoid perturbations, the concentration of the tracer was limited to < 10% or 20% of the substrate concentration, as suggested by previous researchers (Raimbault and Garcia, 2008; Middelburg and Nieuwenhuize, 2000; Painter et al., 2014). One single tracer, $^{15}NH_4^+$, was added to an incubation bottle to trace the ^{15}N flow among the nitrogen pools under simulated *in situ* conditions. Almost all the most fundamental processes in the N cycle can be quantified with this newly proposed method. To demonstrate the applicability of the method, we conducted incubation experiments with low-nutrient water from the western North Pacific and with high-nutrient coastal water off the southeastern China coast. As a result of recent advances in the analytical methods for measuring the concentrations and isotopic compositions of various nitrogen species, we were able to use this isotope matrix method to quantify the *in situ* fluxes of N in the euphotic zone.

2. Isotope matrix method

2.1 Framework of the inter-connections among nitrogen pools

123 Figure 1 shows the transformations of N among NH_4^+, NO_2^-, NO_3^-, PN, and DON
124 in an aerobic euphotic zone. The PN was operationally defined as the particulate
125 organic nitrogen trapped on a GF/F filter (> 0.7 μm). Dissolved inorganic nitrogen
126 (DIN) and DON were equated to the inorganic and organic nitrogen, respectively, in the
127 dissolved fraction that passed through a polycarbonate membrane with a 0.22 μm pore
128 size. Because DON includes the N in numerous dissolved organic N compounds,
129 including unidentified organics, urea, amino acids, amines, and amides, DON
130 represents the "bulk" DON and was calculated by subtracting the concentrations of
131 NH_4^+, NO_2^-, and NO_3^- (DIN) from the total dissolved N (TDN).
132 We used two different models to analyze our data: a low-nutrient model to
133 represent the open ocean and a high-nutrient model to represent estuarine and coastal
134 environments (Fig. 1a and 1b). In the high-nutrient model, NH_4^+, NO_2^-, and NO_3^- were
135 assumed to co-exist. The rationale for the two model structures is as follows.
136 The consumption of reactive inorganic nitrogen (NH_4^+, NO_2^-, and NO_3^-) is
137 dominated by photosynthetic uptake by phytoplankton (F1 and F4 in Fig. 1a; F1, F3,
138 and F5 in Fig. 1b). Heterotrophic bacteria may also play an important role in NH_4^+
139 assimilation (Laws, 1985; Middelburg and Nieuwenhuize, 2000; Veuger et al., 2004).
140 We took heterotrophic bacterial assimilation of NH_4^+ into account as well (F6 in Fig. 1a
141 and F8 in Fig. 1b) to explore its importance. Though NO_2^- may be released during NO_3^-
142 uptake (Lomas and Lipschultz, 2006), little NO_2^- production from NO_3^- was detected
143 by Santoro et al. (2013). Nitrate assimilation may be inhibited in aerobic water,

144 especially in estuaries and coastal seas where the NH_4^+ concentration is high, and in the
145 absence of nitrate uptake, there is no release of nitrite. Thus, nitrite release was ignored
146 in our model. Due to DIN assimilation by phytoplankton, the PN pool may increase,
147 but DON may be released during assimilation (F5 in Fig. 1a and F7 in Fig. 1b) as noted
148 by Bronk et al. (1994), Bronk and Ward (2000), and Varela et al. (2005). The size of
149 the NH_4^+ pool is increased by remineralization (F2 in both Fig. 1a and 1b) and
150 decreased by nitrification. The latter consists of two basic steps: ammonium oxidation
151 by archaea/bacteria (AOA/AOB) to nitrite (F4 in Fig. 1b) and nitrite oxidation to nitrate
152 by nitrite-oxidizing bacteria (NOB) (F6 in Fig. 1b). Although recent studies have
153 revealed a single microorganism that can completely oxidize NH_4^+ to NO_3^-
154 (comammox) (Daims et al., 2015; van Kessel et al., 2015), the importance of
155 comammox in the marine environment remains unclear.

156 Specific mechanisms or processes such as grazing and viral lysis may alter the
157 concentrations of NH_4^+, nitrite, and DON. However, the scope of this study is to
158 determine the nitrogen fluxes among the often-measured and operationally defined
159 nitrogen pools. The organisms that mediate the relevant fluxes are not specifically
160 included in the model. Thus, the results of specific process such as grazing and viral
161 lysis have been incorporated into the paradigm depicted in Fig. 1.

162 **2.2 Analytical methods to determine the amounts of $^{15}N/^{14}N$ in various pools**

163 To trace the ^{15}N movement among pools, our isotope matrix method couples the
164 ^{15}N-labeling and inventory methods by considering changes of both concentrations and

165 isotopic compositions. Analytical methods to determine the concentrations and isotopic
166 compositions of both high and low levels of inorganic/organic nitrogen are in most
167 cases well established and have been reported elsewhere. We determined all the
168 relevant concentrations and isotopic compositions with the exception of the isotopic
169 composition of NH_4^+.

170 Concentrations of NH_4^+ higher than 0.5 μM were measured manually by using the
171 colorimetric phenol hypochlorite technique (Koroleff, 1983). Nanomolar NH_4^+
172 concentrations were measured by using the fluorometric o-phthaldialdehyde (OPA)
173 method (Zhu et al., 2013). Concentrations of NO_2^- and of NO_x^- (NO_2^- + NO_3^-) were
174 determined with the chemiluminescence method following the protocol of Braman and
175 Hendrix (1989). The detection limits of NO_2^- and NO_x^- were both ~ 10 nmol L^{-1}, and
176 the corresponding relative precision was better than 5% within the range of
177 concentrations that we measured. By using persulfate as an oxidizing reagent, we
178 oxidized TDN and PN separately to nitrate (Knapp et al., 2005) and then measured the
179 nitrate by using the analytical method for NO_x^- described above.

180 We determined the $\delta^{15}N$ of NO_2^- with the azide method by following the detailed
181 procedures in McIlvin and Altabet (2005). The $\delta^{15}N$ of NO_x^- was determined by using a
182 distinct strain of bacteria that lacked N_2O reductase activity to quantitatively convert
183 NO_x^- to nitrous oxide (N_2O), which we then analyzed by IRMS (denitrifier method;
184 (Sigman et al., 2001; Casciotti et al., 2002). The isotopic composition of NO_3^- was
185 determined from isotope mass balance (NO_x^- minus NO_2^-) or measured by the

186 denitrifier method after eliminating preexisting NO_2^- with sulfamic acid (Granger and
187 Sigman, 2009). To determine the $\delta^{15}N$ of TDN and PN, both species were first
188 converted to NO_3^- with the denitrifier method, and then the $\delta^{15}N$ of the NO_3^- was
189 determined as described above. The detection limit of $\delta^{15}N_{PN}$ can be reduced to the
190 nanomolar level (absolute amount of nitrogen), which is significantly lower than the
191 detection limit using high temperature combustion with an elemental analyzer
192 connected to IRMS.

193 The most popular way to determine the N isotopic composition of NH_4^+ is the
194 "diffusion method", which involves conversion of dissolved NH_4^+ to NH_3 gas by
195 raising the sample pH to above 9 with magnesium oxide (MgO) and subsequently
196 trapping the gas quantitatively as $(NH_4)_2SO_4$ on a glass fiber (GF) filter; the isotope
197 ratios of the $^{15}N/^{14}N$ are then measured using an elemental analyzer coupled with an
198 IRMS (Holmes et al., 1998; Hannon and Böhlke, 2008). Alternatively, after removing
199 the preexisting NO_2^- from the seawater samples using sulfamic acid, NH_4^+ is first
200 quantitatively oxidized to NO_2^- by hypobromite (BrO^-) at pH ~12 (BrO^- oxidation
201 method), and the protocol of McIlvin and Altabet (2005) is then used to reduce the
202 NO_2^- to N_2O (Zhang et al., 2007). Unfortunately, neither of these methods has been
203 established in our lab yet. The isotope matrix method requires the isotopic composition
204 of NH_4^+ as well, but this requirement can be circumvented by making certain
205 assumptions, as illustrated in our case studies below.

We estimated the amount of ^{14}N and ^{15}N atoms in every individual pool for which we knew the concentration and $\delta^{15}N$ ($\delta^{15}N$ ‰ = $[(R_{sample} - R_{atmN2})/R_{atmN2}] \times 1000$). By assuming the ^{15}N content of standard atmospheric nitrogen to be 0.365% (Coplen et al., 1992), we calculated R_{sample} ($^{15}N/^{14}N$). By defining r_{sample} as $^{15}N/(^{14}N+^{15}N)$, we directly derived the ^{15}N and ^{14}N concentrations of all forms of N, with the exception of NH_4^+ and DON. The r value of the NH_4^+ was assumed to equal either its initial value or an arbitrarily chosen fraction thereof, and the ^{15}N and ^{14}N content of the NH_4^+ was then determined.

2.3 Formation of matrix equations

In this isotope matrix method, we added a limited amount of $^{15}NH_4^+$ into incubation bottles at the very beginning and then monitored the changes of ^{15}N and ^{14}N in the measured pools every few hours. We assumed isotopic mass balance at every time point in the incubation bottle. In other words, the sum of the variations in the total N, ^{15}N, and ^{14}N concentrations were zero for any time interval. The fluxes of ^{15}N and ^{14}N were therefore equal to the total flux multiplied by $r_{substrate}$ and $(1 - r_{substrate})$, respectively. Although we did not consider isotope fractionation, it could have been introduced into the equations by dividing the ^{14}N flux by the ratio of the specific rate constants of ^{14}N and ^{15}N to obtain the flux of ^{15}N.

According to mass balance, the net changes of the ^{15}N (or ^{14}N) concentration of an individual N pool in a time interval are determined by the inflow and outflow of ^{15}N (or ^{14}N) (see Fig. 1 and Eqs. 1–14 below). In the low-nitrogen case, the changes of the

^{15}N concentrations of the NH_4^+, NO_x^-, and PN pools were expressed by Eq. 1, 2, and 3, respectively. Similarly, the temporal dependence of ^{14}N-NH_4^+, ^{14}N-NO_x^-, and ^{14}N-PN were expressed by Eq. 4, 5 and 6, respectively. The mean rate of change of the nitrogen pool, i.e. the left side of each equation, was determined from the data at time zero (t0) and the first time point (t1). For example, when the sampling time interval was short, $\Delta[^{14}NH_4^+]/\Delta t$ at the first time point was approximately $\{[^{14}NH_4^+]_{t1} - [^{14}NH_4^+]_{t0}\}/(t1 - t0)$ where the subscripts indicate the times at which the concentrations were measured. The r value in each equation was the average of the r values for the pool at time zero and the first time point.

$$\frac{\Delta\left[{}^{15}NH_4^+\right]}{\Delta T} = \overline{F_2} \times 0.00366 - \overline{F_1} \times \overline{r_{NH_4^+}} - \overline{F_3} \times \overline{r_{NH_4^+}} - \overline{F_6} \times \overline{r_{NH_4^+}} \quad (1)$$

$$\frac{\Delta\left[{}^{15}NO_x^-\right]}{\Delta T} = \overline{F_3} \times \overline{r_{NH_4^+}} - \overline{F_4} \times \overline{r_{NO_x^-}} \quad (2)$$

$$\frac{\Delta\left[{}^{15}PN\right]}{\Delta T} = \overline{F_1} \times \overline{r_{NH_4^+}} + \overline{F_4} \times \overline{r_{NO_x^-}} - \overline{F_5} \times \overline{r_{PN}} \quad (3)$$

$$\frac{\Delta\left[{}^{14}NH_4^+\right]}{\Delta T} = \overline{F_2} \times (1 - 0.00366) - \overline{F_1} \times (1 - \overline{r_{NH_4^+}}) - \overline{F_3} \times (1 - \overline{r_{NH_4^+}}) - \overline{F_6} \times (1 - \overline{r_{NH_4^+}}) \quad (4)$$

$$\frac{\Delta\left[{}^{14}NO_x^-\right]}{\Delta T} = \overline{F_3} \times (1 - \overline{r_{NH_4^+}}) - \overline{F_4} \times (1 - \overline{r_{NO_x^-}}) \quad (5)$$

$$\frac{\Delta\left[{}^{14}PN\right]}{\Delta T} = \overline{F_1} \times (1 - \overline{r_{NH_4^+}}) + \overline{F_4} \times (1 - \overline{r_{NO_x^-}}) - \overline{F_5} \times (1 - \overline{r_{PN}}) \quad (6)$$

The time series in this study lasted for 24 hours. However, we used only the first two time points for the rate calculations because we felt those rates would be closest to the instantaneous *in situ* rates of the original samples. Although the isotope matrix method may be applied to longer time intervals, rates may vary as a result of substrate consumption and/or community change. Relatively short-term incubations are therefore advisable (see below).

Because the total number of equations and unknowns are equal, a unique solution can be obtained via matrix inversion for the low-nutrient model.

In high-nutrient cases, analogous equations (Eqs. 7–14) can be constructed to describe the fluxes between NH_4^+, NO_2^-, NO_3^-, and PN (Fig. 1b).

$$\frac{\Delta\left[{}^{15}NH_4^+\right]}{\Delta T} = \overline{F_2} \times 0.00366 - \overline{F_1} \times \overline{r_{NH_4^+}} - \overline{F_4} \times \overline{r_{NH_4^+}} - \overline{F_8} \times \overline{r_{NH_4^+}} \quad (7)$$

$$\frac{\Delta\left[{}^{15}NO_2^-\right]}{\Delta T} = \overline{F_4} \times \overline{r_{NH_4^+}} - \overline{F_3} \times \overline{r_{NO_2^-}} - \overline{F_6} \times \overline{r_{NO_2^-}} \quad (8)$$

$$\frac{\Delta\left[{}^{15}NO_3^-\right]}{\Delta T} = \overline{F_6} \times \overline{r_{NO_2^-}} - \overline{F_5} \times \overline{r_{NO_3^-}} \quad (9)$$

$$\frac{\Delta\left[{}^{15}PN\right]}{\Delta T} = \overline{F_1} \times \overline{r_{NH_4^+}} + \overline{F_3} \times \overline{r_{NO_2^-}} + \overline{F_5} \times \overline{r_{NO_3^-}} - \overline{F_7} \times \overline{r_{PN}} \quad (10)$$

$$\frac{\Delta\left[{}^{14}NH_4^+\right]}{\Delta T} = \overline{F_2} \times (1 - 0.00366) - \overline{F_1} \times (1 - \overline{r_{NH_4^+}}) - \overline{F_4} \times (1 - \overline{r_{NH_4^+}}) - \overline{F_8} \times (1 - \overline{r_{NH_4^+}}) \quad (11)$$

$$\frac{\Delta\left[{}^{14}NO_2^-\right]}{\Delta T} = \overline{F_4} \times (1 - \overline{r_{NH_4^+}}) - \overline{F_3} \times (1 - \overline{r_{NO_2^-}}) - \overline{F_6} \times (1 - \overline{r_{NO_2^-}}) \quad (12)$$

258 $$\frac{\Delta\left[{}^{14}NO_3^-\right]}{\Delta T} = \overline{F_6} \times (1 - \overline{r_{NO_2^-}}) - \overline{F_5} \times (1 - \overline{r_{NO_3^-}}) \quad (13)$$

259 $$\frac{\Delta\left[{}^{14}PN\right]}{\Delta T} = \overline{F_1} \times (1 - \overline{r_{NH_4^+}}) + \overline{F_3} \times (1 - \overline{r_{NO_2^-}}) + \overline{F_5} \times (1 - \overline{r_{NO_3^-}}) - \overline{F_7} \times (1 - \overline{r_{PN}}) \quad (14)$$

260 A unique solution can again be obtained via matrix inversion because the number
261 of equations and unknowns are equal.

262 In the above matrix equations, the value of r_{NH4+}, which we did not measure in this
263 study, was needed to obtain a solution. To address this issue, we assumed various
264 degrees of remineralization to test the effect of isotope dilution (NH_4^+ addition) on our
265 calculated fluxes. We reduced r_{NH4+} values of the 24-h incubation. The r_{NH4+} for
266 remineralization (F2) was assumed to be constant (0.00366) and equal constant rates
267 that led to total reductions of r_{NH4+} by 0%, 1%, 10%, 20%, or 50% by the end. The value
268 of F2 coupled with the assumed r_{NH4+} values allowed us to resolve rates under different
269 remineralization scenarios, and the derived F2 was introduced into a STELLA model
270 for extrapolation purposes (see below). We compared the observed and
271 remineralization-associated simulations to elucidate the effect of remineralization on
272 the calculated rates for the time series incubations.

273 **2.4 Validation by STELLA**

274 The initial rates are of particular interest because they are presumably most similar
275 to the *in situ* rates at the time the sample was collected. The initial rate is here
276 distinguished from rates derived from incubations that extended beyond time point t1.

277 To evaluate the applicability of the matrix-derived initial rate, we used STELLA 9.1.4
278 software (Isee systems, Inc.) to construct box models that were consistent with the
279 scenarios depicted in Fig. 1. The constructed STELLA model contained two modules
280 (Figs. S1 and S2), one for ^{15}N and the other for ^{14}N. These two modules were connected
281 through the ^{15}N atom % (rN), which was a parameter measured in the incubation
282 experiment. A model run was initialized with the measured values of the nitrogen pools
283 at time zero, and the model then projected the values of those pools as a continuous
284 function of time. Because the rates based on the first two time points might not
285 accurately represent the behavior of the system throughout the full time course due, for
286 example, to changes in substrate concentrations and the composition of the microbial
287 community, this extrapolation using the initial rates amounted to a test of the
288 hypothesis that the rates did not change.

289 We assumed first-order reaction kinetics in both the low-nutrient and high-nutrient
290 cases. The initial rate constant "k" could therefore be derived by dividing the
291 matrix-derived flux F by $\bar{C}$, the average substrate concentration during the first two
292 time points. After the concentrations of ^{15}N and ^{14}N were initialized in every pool, the
293 model ran for 24 h using the matrix-derived short-term k values. As depicted in Fig. 1,
294 all the monitored N pools were regulated by F, which was assumed to be concentration
295 dependent (Figs. S1 and S2). The output of the model included the time courses of the
296 ^{15}N and ^{14}N concentrations and the ^{15}N atom % (r_N) of each N species. Through this

297 analysis, we could observe the temporal evolution of the isotopic composition of the
298 various N pools.

299 **2.5 Study sites and incubation experiments**

300 The incubation experiments were conducted in two environments with very
301 different nutrient levels. The low-nutrient study was conducted on-deck of the R/V
302 Dongfanghong 2 on a cruise to the Western North Pacific (WNP) (33.3 °N, 145.9 °E) in
303 the spring of 2015. The site of the high-nutrient study was Wuyuanwan Bay (WYW)
304 (24.5 °N, 118.2 °E) in the southern coast of China.

305 The water samples at the WNP station were collected using a 24-bottle rosette
306 sampler. The sampling depth was 25 m, at which the light intensity was 12% of the
307 surface irradiance. Two pre-washed 10-L polycarbonate carboys (Nalgene, USA) were
308 used for the incubation. A total of 1.5 mL of 200 μM ^{15}N-labeled NH_4Cl tracer
309 containing 98 atom % ^{15}N (Sigma-Aldrich, USA) was injected into each incubation
310 bottle separately to achieve a final concentration of 30 nM. The incubation was carried
311 out immediately with a constant simulated light intensity of 35 μmol photons m^{-2} s^{-1} in
312 a thermostatic incubator (GXZ-250A, Ningbo) at the *in situ* temperature.

313 The WYW station was located in the inner bay, where the tide was semidiurnal.
314 Wuyuanwan, a coastal bay, suffers from the same anthropogenic influences that cause
315 eutrophication in other coastal areas of China. However, the bay water is well
316 ventilated and constantly saturated with dissolved oxygen due to tidally induced water

exchange. It is an ideal site to study the dynamic transformations that characterize the coastal nitrogen cycle.

The WYW samples were taken on 19 January 2014 from water depths of 0.3 m and 2.3 m, where the light intensities were 80% and 2%, respectively, of the surface water irradiance. Duplicate water samples were collected from each depth by using submersible pump to fill pre-washed 10-L polycarbonate bottles (Nalgene, USA). ^{15}N-labeled NH_4Cl (98 atom % ^{15}N, Sigma-Aldrich, USA) was added to the incubation bottles to a final concentration of 1 μM (~4% of the ambient concentration). The incubations were carried out immediately in the field. Neutral density screens that allowed 80% and 2% light penetration were used to simulate the light intensities at 0.3 m and 2.3 m, respectively. The temperature was maintained at ~13.7 ℃ by continuously pumping seawater through the incubators.

The sample at the first time point (t0) was taken immediately after tracer addition. Subsequent samples were taken at approximately 2–4 h intervals for DIN and PN analyses. An aliquot of 200 mL was filtered through a 47-mm polycarbonate membrane filter with a 0.22 μm pore size (Millipore, USA). The filtrates were frozen at –20 ℃ for chemical analyses in the lab. Particulate matter was collected by filtering 500 ml seawater through pre-combusted (450 ℃ for 4 h) 25 mm GF/F filters (Whatman, GE Healthcare, USA) at a pressure of <100 mm Hg. The GF/F filters were freeze-dried and stored in a desiccator prior to analysis of PN concentrations and ^{15}N atom %.

3. Results

3.1 Ambient conditions and initial concentrations

The water temperature and salinity at a depth of 25 m in the WNP were 18.4 ℃ and 34.8, respectively. The dissolved oxygen (DO) was 7.3 mg L^{-1}. The concentrations of NH_4^+, NO_x^-, and phosphate were 113 ± 5 nmol L^{-1}, 521 ± 18 nmol L^{-1} and 74 ± 2 nmol L^{-1}, respectively.

The water temperature and salinity throughout the water column of the WYW were 13.5 ± 0.1 ℃ and 29.5 ± 0.1, respectively. The DO saturation fell in the range 135–140%. The concentrations of nitrogenous species were relatively high. The inorganic nutrient concentrations were 30.9 ± 0.7 μmol L^{-1} for NO_3^-, 22.3 ± 4.3 μmol L^{-1} for NH_4^+, 5.4 ± 0.2 μmol L^{-1} for NO_2^-, and 1.5 ± 0.1 μmol L^{-1} for phosphate. The PN concentration was 9.3 ± 0.7 μmol L^{-1}.

3.2 Time-courses of incubations

3.2.1 Low nutrient case in the WNP

The observed patterns of change of the bulk NH_4^+, NO_x^-, PN, and TDN concentrations and the $\delta^{15}N$ of NO_x^- and PN during the incubation are shown in Figure 2. Concentrations of NH_4^+ and NO_x^- decreased rapidly from 143 ± 5 to 48 ± 5 nM and 521 ± 18 to 127 ± 11 nM, respectively (Figs. 2a and 2b). In contrast, the PN concentration increased from 437 ± 9 to 667 ± 14 nM (Fig. 2c), and the TDN concentration remained stable, with an average of 6511 ± 209 nM (Fig. 2d). In contrast to the trend of NO_x^- concentration, $\delta^{15}N$-NO_x^- increased from 8.9 ± 0.2 to 171 ± 2 ‰

(Fig. 2e). In addition, δ^{15}N-PN exhibited great changes, increasing from 46.8 ± 0.2 to 6950 ± 314 ‰ (Fig. 2f).

3.2.2 High nutrient case in the WYW

The time-series of observational parameters for samples from depths of 80% and 2% of surface PAR (sPAR) exhibited similar trends during the incubation (Fig. 3). During the course of the incubation, NH_4^+ decreased significantly and continuously from 26.6 ± 0.1 (initial concentration) to 17.4 ± 0.1 μmol L^{-1}. The mean reduction rate was 0.63 μmol L^{-1} h^{-1} for the 80% sPAR sample (Fig. 3a). The NH_4^+ concentration of 2% sPAR sample decreased more slowly from 24.6 ± 0.1 (initial concentration) to 18.2 ± 1.0 μmol L^{-1} with a mean reduction rate of 0.47 μmol L^{-1} h^{-1} (Fig. 3a). NO_3^- in 80% and 2% sPAR samples decreased from 30.1 ± 0.1 to 28.3 ± 0.1 μmol L^{-1} and from 31.1 ± 0.1 to 29.7 ± 0.1 μmol L^{-1}, respectively (Fig. 3c). Overall, the nitrate reduction rates were much lower than the NH_4^+ reduction rates. Compared to nitrate, NO_2^- displayed even slower rates of decline, yet the rate was significantly higher at 80% sPAR than at 2% sPAR (Fig. 3b). Similar to the low nutrient case, PN increased steadily from 8.8 ± 0.1 to 17.7 ± 0.9 μmol L^{-1}, with a mean rate of 0.61 μmol L^{-1} h^{-1} at 80% sPAR and from 9.9 ± 0.1 to 16.0 ± 2.0 μmol L^{-1} with a mean rate of 0.44 μmol L^{-1} h^{-1} at 2% sPAR (Fig. 3d). The rates of increase of the PN concentration were very close to the rates of decrease of NH_4^+, the indication being that ammonium was the major nitrogen source for growth. The TDN concentration decreased from 78.7 ± 1.6 to 68.4 ± 0.1 μmol L^{-1} and from 72.8 ± 2.5 to 67.1 ± 0.8 μmol L^{-1} at 80% and 2% sPAR, respectively (Fig. 3e).

The $\delta^{15}N\text{-}NO_2^-$ increased from –9.0 ± 0.1 to 12.1 ± 0.1 ‰ and from –8.8 ± 0.1 to 23.3 ± 0.6 ‰ at 80% and 2% sPAR, respectively (Fig. 3g). Because the nitrate pool was relatively large, the values of $\delta^{15}N\text{-}NO_3^-$ ranged from 6.8 to 10.1 ‰ with no significant trend over time (Fig. 3h). In addition, $\delta^{15}N$-PN increased from 14.8 ± 0.3 to 3078 ± 180 ‰ and from 15.0 ± 0.5 to 2738 ± 66 ‰ at 80% and 2% sPAR, respectively (Fig. 3i). These significant changes in both the concentration and isotopic composition of the nitrogen pools over time suggests that there were significant movements of nitrogen among pools and that the labeled ^{15}N in the NH_4^+ moved throughout the system, with the exception of nitrate.

3.3 Solutions of the matrix equation and STELLA extrapolation

3.3.1 Low nutrient case

The matrix-derived rate constants (ki) and rates (Fi) are shown in Table 1(A) and 1(B), respectively. Under the no remineralization condition (i.e. r_{NH4+} decreased 0% within 24 hours), NO_x^- uptake (k4 = 0.059 h^{-1}; F4 = 27.2 nmol L^{-1} h^{-1}) was the highest among all forms of inorganic nitrogen in terms of flux, followed by NH_4^+ uptake (k1 = 0.038 h^{-1}; F1 = 4.9 nmol L^{-1} h^{-1}) and DON release (k5= 0.024 h^{-1}; F5 = 11.5 nmol L^{-1} h^{-1}). NH_4^+ uptake by bacteria (k6 = 0.007 h^{-1}; F6 = 1.0 nmol L^{-1} h^{-1}) was much lower than that by phytoplankton. The rate constant for nitrification (k3 = 0.0005 h^{-1}) was the lowest among all fluxes (F3 = 0.07 nmol L^{-1} h^{-1}).

By introducing the initial ^{15}N and ^{14}N concentrations of NH_4^+, NO_x^-, PN, and DON and the calculated rate constants (k1 to k6) into STELLA (Fig. S1), we obtained a

400 full time courses for all parameters (Fig. 4). Generally, the model outputs fitted well
401 with the measured values, except for the last time point for PN, the associated ^{15}N
402 concentration, $\delta^{15}N$, and r_N (Figs. 4 c, k and o). The fact that the rates during the first
403 time interval generally predicted rather well the subsequent observations demonstrated
404 a good predictive performance with the matrix method initial rate. Because the
405 concentrations of both ammonium and NO_x^- were described well during the 24-h
406 experiment, the extra PN that was not well described in observations after 12 hours
407 likely reflected the influence of an additional nitrogen source, i.e., dissolved organic
408 nitrogen that was utilized by phytoplankton (see discussion below) when inorganic
409 nitrogen reached threshold levels (Sunda and Ransom, 2007).

410 In the test runs with r_{NH4+} reduction by a total of 1%, 10%, 20% and 50%, we
411 found that the NH_4^+ consumption rates (k1 and k6) increased as the regeneration (k2)
412 increased (Table 1). As indicated in previous studies, such regeneration-induced
413 isotope dilution indeed altered the original results (Table 1 and Fig. 4). Specifically,
414 greater NH_4^+ regeneration resulted in larger differences between the three
415 PN-associated values (^{15}N-PN, $\delta^{15}N$-PN, and r_{PN}) and the STELLA-projected data
416 (Figs. 4 c, k and o). The dilution effect was more significant after 12 hours of
417 incubation. In contrast, the effect of r_{NH4+} on parameters associated with NO_x^- was
418 trivial (Figs. 4 b, f, j, n and r). The comparison between the simulation and observation
419 suggested that NH_4^+ regeneration needs to be considered for PN (i.e., uptake) when the
420 remineralization rate is high and the incubation is longer than 12 hours. Besides

421 remineralization, discrepancies along the time course might possibly be caused by
422 changes in the composition of the microbial community as the incubation continues.

423 **3.3.2 High nutrient cases**

424 The results at 80% sPAR and 2% sPAR on the assumption of a fixed r_{NH4+} are
425 shown in Table 2(A) and 2(B), respectively. For the 80% sPAR sample, the NH_4^+
426 uptake by phytoplankton (F1, 397 nmol L^{-1} h^{-1}) and by bacteria (F8, 282 nmol L^{-1} h^{-1})
427 were much higher than the other rates and were followed by the NO_3^- uptake rate (F5,
428 149 nmol L^{-1} h^{-1}). The NO_2^- uptake (F3) rate was 29 nmol L^{-1} h^{-1}, much lower than that
429 of NH_4^+ and NO_3^-. The ammonia oxidation rate (F4) was 0.4 nmol L^{-1} h^{-1}, and the
430 nitrite oxidation rate (F6) was zero (Table 2A). Because this incubation was conducted
431 in winter with low temperature and at 80% sPAR, low rates of ammonium and nitrite
432 oxidation were reasonable because both nitrifiers and NOB are sensitive to light (e.g.
433 Olson, 1981a, 1981b; Horrigan et al., 1981; Ward, 2005; Merbt et al., 2012; Smith et al.,
434 2014). The DON release rate by phytoplankton (F7) was zero in this case.

435 In comparison, all the rates at 2% sPAR showed a very similar pattern (Table 2B).
436 The only difference was that all the uptake rates were lower at 2% sPAR, except for
437 ammonia oxidation, which was higher in the low light.

438 By introducing initial concentrations and calculated rate constants (k1–k8) into the
439 STELLA model (Fig. S2), we obtained a time series of ^{15}N and ^{14}N concentrations and
440 the r_N values for NH_4^+, NO_2^-, NO_3^-, PN and DON (Fig. 5). In general, the modeled and

441 measured values remained consistent throughout the 15-h incubation, demonstrating
442 the capability of the isotope matrix method.

443 Similar to the low-nutrient case, we evaluated the effect of regeneration (see Table
444 2 and Fig. 5A and 5B). Because ammonium uptake was the dominant process, changes
445 of the PN pool were more significant in comparison with the other pools (Figs. 5 d, n
446 and s). We found again that as F2 increased, F1 and F8 increased to maintain a constant
447 reduction of the measured NH_4^+ concentration (Table 2). Similar to the low-nutrient
448 case, as regeneration increased, the projected course of ^{15}N-PN deviated more from
449 observations, and the turning point also appeared earlier, resulting in a larger curvature
450 of r-PN and δ^{15}N-PN (Fig. 5d and 5s). This modeling exercise confirmed the influence
451 of the isotope dilution effect. However, the effect was insignificant in the early part of
452 the incubation.

453 # 4. Discussion

454 ## 4.1 Method comparisons

455 ### 4.1.1 Model structure and rate derivation

456 The most widespread ^{15}N model was proposed by Dugdale and Goering (1967),
457 who assumed isotopic and mass balances in the particulate fraction, the result being the
458 commonly used equation for nitrogenous nutrient uptake. Dugdale and Wilkerson
459 (1986) modified their rate equations further and highlighted the importance of
460 short-term incubations. Collos (1987) demonstrated that an equation based on the

concentration of particles at the end of the experiment, rather than at the beginning, was more reliable when more than one N source was simultaneously incorporated by the phytoplankton. That is, the equation by Collos (1987) corrected for the bias caused by use of unlabeled multiple N sources.

Unlike the above-mentioned equations, Blackburn (1979) and Caperon et al. (1979) proposed ^{15}N isotope dilution models based on the substrate rather than the product. By measuring the isotope values and concentrations of the substrate (e.g. NH_4^+), both NH_4^+ consumption (DON and/or PN as product) and regeneration rates can be obtained. Glibert et al. (1982) further modified the isotope dilution method and calculated the uptake rate into the PN fraction by substituting the exponential average of r_{NH4+} at the beginning and at the end of an incubation to correct for the isotope dilution in the model of Dugdale and Goering (1967). Despite the methodological improvements, imbalance was often observed between the substrate reduction and the increase in the particulate phase in field studies. Laws (1985) introduced a new model that considered the imbalance and calculated the "net uptake rate" (into PN). Later on, Bronk and Glibert (1991) revised Laws' model on the basis of the model proposed by Glibert et al. (1982) to calculate the "gross uptake rate" (substrate incorporation into particulate organic nitrogen plus DON). None of the above models considered the mass balance at the whole system scale. Although rates were obtained via analytical solutions, the bias potential due to multiple fluxes was not completely resolved.

481 To address this problem, Elskens et al. (2002) formulated a new model that takes
482 into account multiple co-occurring N fluxes in a natural system. The model contains
483 3n + 1 equations and an equal number of flux rates, where n is the number of labeled
484 N substrates. The rates in their model were estimated using a weighted least squares
485 technique. Elskens et al. (2005) subsequently created a process-oriented model
486 (PROM) that accounted for as many N processes as needed to quantify how specific
487 underlying assumptions affected the behavior of the estimates of all the
488 above-mentioned models. The authors concluded that uncertainties may increase as
489 the incubation is prolonged and that oversimplified models may risk bias when their
490 underlying assumptions are violated. The most recent attempt to resolve simultaneous
491 N processes was conducted by Pfister et al. (2016), who used parallel incubations (^{15}N
492 labeled NH_4^+ and NO_3^-) in tidepools to measure multiple flows among benthic N,
493 ammonium, nitrite, and nitrate. In their experiment, six differential equations were
494 constructed based on mass and isotope balances and solved by using the ODE
495 function of the R language. Because the N content of benthic algae was not measured
496 due to sampling difficulties and spatial heterogeneity of biomass, a mass balance at
497 the whole system scale could not be achieved. Specifically, the rate of DON release
498 could not be determined.

499 Compared with the methods or models mentioned above, the advantages of the
500 isotope matrix method include (1) the potential biases caused by multiple flows were
501 taken into consideration subject to the constraint that there be a mass balance at the

system level; (2) one tracer addition was sufficient to quantify multiple *in situ* flows; parallel incubations, i.e., light and dark or $^{15}NH_4^+$ and $^{15}NO_x^-$, were not needed; (3) post-hoc data processing was simple, and a unique solution can be obtained via matrix inversion; (4) no extra laboratory work was necessary (see below).

4.1.2 Rate comparisons

In accord with Pfister et al. (2016), we estimated all N transformation rates using ordinary differential equations (ODEs) for the three cases on the assumption that r_{NH4+} was constant (see Table 1−3). In general, the rates obtained by matrix inversion and integration of the ODEs were consistent. Differences, when apparent, were caused by the duration of the integration. The isotope matrix method was applied to only the first two time points (i.e., time intervals of either 2 or 4 hours), whereas the ODEs were integrated for the entire 24-h incubation. In Pfister et al. (2016), ODEs were used to analyze data collected at 3 time points within a 5-h time interval. Unfortunately, such intensive sampling for on-deck incubations is not practical. However, we strongly recommend short-term incubations for water column studies. Two time points separated by a few hours may be more convenient and realistic for instantaneous rate estimates.

Below, we present a comparison between our results and conventional source-product rate measurements (Collos, 1987) of ammonium oxidation and uptake (Table 3). The matrix-derived NH_4^+ uptake rates for all of the experiments were consistent with the rates (difference < 8%) from the traditional source-product method

523 when the final PN concentration was used in the calculation. The fact that the
524 deviations were larger (13−21%) when the initial PN was used is consistent with the
525 conclusions of previous studies that estimates involving the final PN concentration are
526 more reliable. The deviation could obviously be higher if the phytoplankton growth
527 rate was higher.

528 In contrast, the end-products of ammonium oxidation or nitrification are
529 consumed by phytoplankton continuously in the euphotic zone. In many cases, nitrate
530 uptake has been shown to occur in both the light and dark (e.g. Dugdale and Goering,
531 1967; Lipschultz, 2002; Mulholland and Lomas, 2008). The significant consumption of
532 end-products (NO_x^- and NO_2^-) violates the assumption that underlies the
533 source-product rate calculation. Therefore, the NH_4^+ oxidation/nitrification rate cannot
534 be determined with a source-product model. Although phytoplankton consumption
535 resulted in a net reduction of NO_x^- in all of our experiments, we were nevertheless able
536 to determine NH_4^+ oxidation/nitrification rates with the isotope matrix method (Figs.
537 2b, 3b, and 3c) (see Table 3).

538 In most previous studies, the final isotopic composition but not the final
539 concentration of NO_x^- has been measured. As a result, researchers may not have been
540 aware that the outflow of $^{15}NO_x^-$ was greater than the inflow. During dark incubations,
541 researchers may also assume insignificant NO_x^- consumption. However, a "net
542 decrease in end-product" is almost unavoidable when an incubation is conducted
543 under simulated *in situ* light conditions to estimate ammonium oxidation. To address

this consumption effect, Santoro et al. (2010, 2013) took NO_x^- removal into account and formulated a new equation that took account of the nitrification rate (F) and NO_x^- uptake rate (k). In accord with Santoro et al. (2010), we calculated the nitrification rate for the low-nutrient case via a nonlinear least-squares curve-fitting routine in Matlab by using the first three time points of the $^{15}N\text{-}NO_x^-$ /$^{14}N\text{-}NO_x^-$ measurements. The calculated rate, 0.05 nmol L^{-1} h^{-1} (Table 3), was ~30% lower than the matrix-derived rate of 0.07 nmol L^{-1} h^{-1}. In contrast, the nitrate uptake rate constant ($k = 0.010\ h^{-1}$) was only one-sixth of the rate constant (0.059 h^{-1}) derived from the matrix method, although a comparable nitrification rate was obtained when the consumption term was taken into account.

Surprisingly, when we introduced the values of F and k determined with the method of Santoro et al. (2010) into STELLA to generate time courses of variables, we found that the simulated values of $\delta^{15}NO_x^-$ and r_{NOx-} agreed well with those determined by the isotope matrix method (Figs. 4j and 4n). However, much slower decreasing trends were found for $^{15}NO_x^-$, $^{14}NO_x^-$, and NO_x^- (Figs. 4 b, f and r). Finally, we realized that the equation proposed by Santoro et al. (2010) was constrained only by the changes of the ratios rather than by the changes of the individual concentrations of $^{15}NO_x^-$ and $^{14}NO_x^-$. Thus, nonlinear curve-fitting may provide a correct simulation only of the change of the ratio. This conclusion implies that the nitrate uptake rate derived from nonlinear curve-fitting should be validated by the final concentration of nitrate, as was done by Santoro et al. (2013).

In summary, (1) accurate measurements of concentrations during a time series is vital for all kinds of transformation rate estimates, including the isotope matrix method and (2) the isotope matrix method can overcome various biases that impact estimates made with traditional methods.

4.2 Implications for nitrogen biogeochemical processes

Results of use of the isotope matrix method suggest several conclusions with respect to biogeochemical processes.

4.2.1 Remineralization, regeneration, and community succession

The matrix solution was consistent with the model runs with variable r-NH_4^+ at time points of no more than 12 h, the implication being that dilution effects were negligible during the early incubation period, at least in our studies. Dilution effects could be significant when remineralization is intensive and the incubation longer. Pfister et al. (2016) found that macrofauna (mussels) play an important role in remineralization. The fact that zooplankton in our water samples were not abundant might be a reason for the low remineralization rates in our short-term incubations.

In the WNP low-nutrient case, after an incubation of 24 hours, the levels of nitrate and ammonium approached the concentration threshold for phytoplankton utilization (e.g., <30−40 nM NH_4^+ for *Emiliania huxleyi*; Sunda and Ransom, 2007). In Figure 4, the STELLA projection agreed well with the PN concentrations for only the first 12 hours. In this case, we actually observed phytoplankton succession. Our flow

585 cytometry data (Fig. S3) demonstrated that the number of living eukaryotic cells (4
586 times higher than *Synechococcus*) increased in the first 24 hours and started to drop
587 rapidly after 24 hours. In contrast, the growth of *Synechococcus* continued after 24
588 hours, even though nitrogen concentrations dropped to constantly low level. These
589 observations suggest that the phytoplankton community was competing for nitrogen,
590 and a major community shift started at around 24 hours. After the time point at 12 hours,
591 the observed concentrations of ^{14}N and ^{15}N in the PN were higher than those projected
592 by STELLA. The most intriguing phenomenon among PN-associated parameters was
593 the additional ^{15}N, which could not have come from $^{15}NH_4^+$. The most likely source of
594 nitrogen with enriched ^{15}N to support *Synechococcus* growth was the nitrogen released
595 from dead eukaryotes, which contained freshly consumed ^{15}N tracer, rather than the
596 ambient DON. More studies are needed to explore nutrient thresholds for different
597 phytoplankton species. Nevertheless, our results suggest that incubations must last no
598 more than a few hours for nitrogen uptake studies in the oligotrophic ocean.

599 **4.2.2 Evaluation of the contribution of nitrification to new production**

600 Nitrification in the euphotic zone of the ocean drew little attention until recent
601 years after molecular evidence led to the discovery of the widespread occurrence of
602 ammonia oxidizing archaea (AOA) (Francis et al., 2005; Santoro et al., 2010, 2013;
603 Smith et al., 2014) and rate measurements based on isotopic studies (Ward, 2011;
604 Santoro et al., 2010; Grundle et al., 2013; Smith et al., 2014). As mentioned in the
605 Introduction, the conventional "new" production may have been overestimated 19−33%

606 on a global scale due to the nitrate regenerated in the euphotic zone via nitrification.
607 However, a more realistic assessment of the fractional contribution of nitrification to
608 NO_3^- uptake can only be achieved when incubations are conducted in the same bottle
609 under *in situ* light conditions instead of parallel incubations in the dark and light. The
610 isotope matrix method is so far the most convenient and suitable method for evaluating
611 the relative importance of co-occurring nitrification and new production in the euphotic
612 zone. In all our experimental studies, the contributions of nitrification to new
613 production were < 1% (Table 4). This relatively low contribution was probably due to
614 light inhibition of nitrifiers in the WNP and the low water temperature.

615 Nevertheless, light effects in our studies were significant. Light suppresses
616 nitrification (Ward, 2005; Merbt et al., 2012; Peng et al., 2016). The NH_4^+ oxidation
617 rate at 80% sPAR was reduced by 36% relative to the rate at 2% sPAR. These results
618 are consistent with current knowledge, although some recent evidence has shown that
619 some taxa of marine AOA have the genetic capability to reduce oxidative stress and to
620 repair ultraviolet damage (Luo et al., 2014; Santoro et al., 2015). More case studies
621 are needed in the future to explore the vertical distribution of the relative contribution
622 of nitrification to new production in the euphotic zone.

623 **4.2.3 Nutrient preference**

624 Phytoplankton use a variety of nitrogenous species for growth. McCarthy et al.
625 (1977) introduced the concept of a relative preference index (RPI) to assess the relative
626 use of different forms of N, and an RPI >1 indicates a preference for the specific

627 substrate over other forms of N. As shown in Table 4, in the low nutrient case NO_3^- was
628 preferred. The fact that the RPI for NO_3^- was slightly higher than the RPI for NH_4^+ was
629 probably due to the phytoplankton community structure, as mentioned above. This
630 result is consistent with studies in the Sargasso Sea (Fawcett et al., 2011). However, in
631 the high-nutrient case, the order of the RPI values was $NH_4^+ > 1 > NO_3^- > NO_2^-$, the
632 suggestion being that phytoplankton preferred NH_4^+ over NO_3^- and NO_2^-, similar to the
633 results of studies in Chesapeake Bay (McCarthy et al., 1977).

634 **4.2.4 Quantifying various ammonium consumption pathways**

635 In the upper ocean, NH_4^+ cycles rapidly due to the metabolic pathways of the
636 various microorganisms that compete for ammonium. Ammonium may serve as a
637 nitrogen source for phytoplankton assimilation, and as an energy source for
638 ammonia-oxidizing organisms (AOM). Moreover, many studies have shown that
639 bacteria also play a part in NH_4^+ utilization (Middelburg and Nieuwenhuize, 2000;
640 Veuger et al., 2004). Our results in the low-nutrient case showed that phytoplankton
641 were the main consumers of NH_4^+ (82% of the total NH_4^+ consumption). Bacteria
642 accounted for another ~17%, and AOM used the remaining 1%. In the high-nutrient
643 study, phytoplankton and bacteria each consumed ~50% of the total NH_4^+ (Table 4).

644 ## 5. Conclusions

645 The isotope matrix method was designed specifically for incubations in the
646 euphotic zone under simulated *in situ* conditions. By considering multiple flows among

pools and requiring mass balance at the whole-system level, we minimized potential biases caused by non-targeted processes in traditional source-product methods. Given the progress in analytical techniques for measuring concentrations and isotopic compositions of nitrogen species, the isotope matrix method is a promising approach for studying of rates of nitrogen fluxes from a system-wide perspective. Furthermore, the matrix method is also appropriate for probing the effects of environmental factors (e.g., CO_2, pH, temperature, and light intensity) on interactive N processes in a single incubation bottle.

Acknowledgement

We sincerely thank Wenbin Zou and Tao Huang at the State Key Laboratory of Marine Environmental Science (Xiamen University, China) for their valuable help with the water sampling and the on-board trace NH_4^+ concentration analysis during the 2015 NWP cruise. Yu-ting Shih from the Department of Geology at National Taiwan University in Taiwan is thanked for his help on ODE application. This research was funded by the National Natural Science Foundation of China (NSFC U1305233, 2014CB953702, 91328207, 2015CB954003).

References

Beman, J. M., Popp, B. N., and Alford, S. E.: Quantification of ammonia oxidation rates and ammonia-oxidizing archaea and bacteria at high resolution in the Gulf of California and eastern tropical North Pacific Ocean, Limnol. Oceanogr., 57, 711-726, doi: 10.4319/lo.2012.57.3.0711, 2012.

Blackburn, T. H.: Method for Measuring Rates of NH_4^+ Turnover in Anoxic Marine Sediments, Using a ^{15}N-NH_4^+ Dilution Technique, Appl. Environ. Microbiol., 37, 760-765, 1979.

Braman, R. S., and Hendrix, S. A.: Nanogram nitrite and nitrate determination in environmental and biological materials by vanadium (III) reduction with chemiluminescence detection, Anal. Chem., 61, 2715-2718, doi: 10.1021/ac00199a007, 1989.

Brauwere, A. D., Ridder, F. D., Pintelon, R., Elskens, M., Schoukens, J., and Baeyens, W.: Model selection through a statistical analysis of the minimum of a weighted least squares cost function, Chemom. Intell. Lab. Syst., 76, 163-173, doi: 10.1016/j.chemolab.2004.10.006, 2005.

Bronk, D., Killberg-Thoreson, L., Sipler, R., Mulholland, M., Roberts, Q., Bernhardt, P., Garrett, M., O'Neil, J., and Heil, C.: Nitrogen uptake and regeneration (ammonium regeneration, nitrification and photoproduction) in waters of the West Florida Shelf prone to blooms of Karenia brevis, Harmful Algae, 38, 50-62, doi: 10.1016/j.hal.2014.04.007, 2014.

Bronk, D. A., and Glibert, P. M.: A ^{15}N tracer method for the measurement of dissolved organic nitrogen release by phytoplankton, Mar. Ecol. Prog. Ser., Marine Ecology Progress, 77, 1991.

Bronk, D, A, and Glibert, P, M.: The fate of the missing ^{15}N differs among marine systems, Limnol. and Oceanogr., 39(1), 189-195, doi: 10.4319/lo.1994.39.1.0189 1994.

Bronk, D. A., Glibert, P. M., and Ward, B. B.: Nitrogen uptake, dissolved organic nitrogen release, and new production, Science, 265, 1843-1846, 1994.

Bronk, D. A., and Ward, B. B.: Magnitude of dissolved organic nitrogen release relative to gross nitrogen uptake in marine systems, Limnol. Oceanogr., 45, 1879-1883, doi: 10.4319/lo.2000.45.8.1879, 2000.

Caperon, J., Schell, D., Hirota, J., and Laws, E.: Ammonium excretion rates in Kaneohe Bay, Hawaii, measured by a ^{15}N isotope dilution technique, Mar. Biol., 54, 33-40, doi: 10.1007/BF00387049, 1979.

Casciotti, K., Sigman, D., Hastings, M. G., Böhlke, J., and Hilkert, A.: Measurement of the oxygen isotopic composition of nitrate in seawater and freshwater using the denitrifier method, Anal. Chem., 74, 4905-4912, 2002.

Casciotti, K. L.: Nitrogen and Oxygen Isotopic Studies of the Marine Nitrogen Cycle, Ann. Rev. Mar. Sci., 8, 379-407, doi: 10.1146/annurev-marine-010213-135052, 2016.

703 Chen, Y.-l. L.: Spatial and seasonal variations of nitrate-based new production and
704 primary production in the South China Sea, Deep Sea Res. Part I Oceanogr. Res. Pap.,
705 52, 319-340, doi: 10.1016/j.dsr.2004.11.001, 2005.

706 Collos, Y.: Calculations of ^{15}N uptake rates by phytoplankton assimilating one or
707 several nitrogen sources, International Journal of Radiation Applications and
708 Instrumentation. Part A. Applied Radiation and Isotopes, 38, 275-282, doi:
709 10.1016/0883-2889(87)90038-4, 1987.

710 Coplen, T. B, Krouse, H. R, and Böhlke, J. K.: Reporting of nitrogen isotope
711 abundances-(Technical report). Pure and Applied Chemistry, 907-908, 1992.

712 Daims, H., Lebedeva, E. V., Pjevac, P., Han, P., Herbold, C., Albertsen, M., Jehmlich,
713 N., Palatinszky, M., Vierheilig, J., Bulaev, A., Kirkegaard, R. H., von Bergen, M.,
714 Rattei, T., Bendinger, B., Nielsen, P. H., and Wagner, M.: Complete nitrification by
715 Nitrospira bacteria, Nature, 528, 504-509, 10.1038/nature16461, doi:
716 10.1038/nature16461, 2015.

717 Dore, J. E., and Karl, D. M.: Nitrification in the euphotic zone as a source for nitrite,
718 nitrate, and nitrous oxide at Station ALOHA, Limnol. Oceanogr., 41(8):1619-1628,
719 1996.

720 Dugdale, R., and Goering, J.: Uptake of new and regenerated forms of nitrogen in
721 primary productivity, Limnol. Oceanogr., 12, 196-206, doi: 10.4319/lo.1967.12.2.0196,
722 1967.

723 Dugdale, R., and Wilkerson, F.: The use of ^{15}N to measure nitrogen uptake in eutrophic
724 oceans; experimental considerations, Limnol. Oceanogr., 31, 673-689, doi:
725 10.4319/lo.1986.31.4.0673, 1986.

726 Elskens, M., Baeyens, W., Cattaldo, T., Dehairs, F., and Griffiths, B.: N uptake
727 conditions during summer in the Subantarctic and Polar Frontal Zones of the Australian
728 sector of the Southern Ocean, J. Geophys. Res.: Oceans, 107, 3-1-3-11, doi:
729 10.1029/2001JC000897, 2002.

730 Elskens, M., Baeyens, W., Brion, N., Galan, S. D., Goeyens, L., and Brauwere, A. D.:
731 Reliability of N flux rates estimated from ^{15}N enrichment and dilution experiments in
732 aquatic systems, Global Biogeochem. Cycles, 19, 573-574, doi:
733 10.1029/2004GB002332, 2005.

734 Falkowski, P. G.: Evolution of the nitrogen cycle and its influence on the biological
735 sequestration of CO_2 in the ocean, Nature, 387, 272-275, doi: 10.1038/387272a0, 1997.

736 Fawcett, S. E., Lomas, M. W., Casey, J. R., Ward, B. B., and Sigman, D. M.:
737 Assimilation of upwelled nitrate by small eukaryotes in the Sargasso Sea, Nature
738 Geoscience, 4, 717-722, doi: 10.1038/ngeo1265, 2011.

739 Francis, C. A., Roberts, K. J., Beman, J. M., Santoro, A. E., and Oakley, B. B.: Ubiquity
740 and diversity of ammonia-oxidizing archaea in water columns and sediments of the
741 ocean, Proceedings of the National Academy of Sciences, 102, 14683-14688, doi:
742 10.1073/pnas.0506625102, 2005.

743 Gilbert, P. M., Lipschultz, F., McCarthy, J. J., and Altabet, M. A.: Isotope dilution
744 models of uptake and remineralization of ammonium by marine plankton, Limnol.
745 Oceanogr., 27, 639-650, 1982.

746 Granger, J., and Sigman, D. M.: Removal of nitrite with sulfamic acid for nitrate N and
747 O isotope analysis with the denitrifier method, Rapid Commun. Mass Spectrom., 23,
748 3753-3762, 10.1002/rcm.4307, doi: 10.1002/rcm.4307, 2009.

749 Grundle, D. S., Juniper, S. K., and Giesbrecht, K. E.: Euphotic zone nitrification in the
750 NE subarctic Pacific: Implications for measurements of new production, Mar. Chem.,
751 155, 113-123, doi: 10.1016/j.marchem.2013.06.004, 2013.

752 Hannon, J. E., and Böhlke, J. K.: Determination of the delta ($^{15}N/^{14}N$) of Ammonium
753 (NH_4^+) in Water: RSIL Lab Code 2898, US Geological Survey 2328-7055, 2008.

754 Harrison, P. J., and Davis, C. O.: Use of the perturbation technique to measure nutrient
755 uptake rates of natural phytoplankton populations, Deep Sea Res., 24, 247-255, doi:
756 10.1016/S0146-6291(77)80003-9, 1977.

757 Harrison, W. G., Harris, L. R., Karl, D. M., Knauer, G. A., and Redalje, D.G.: Nitrogen
758 dynamics at the VERTEX time-series site, Deep Sea Res. Part I Oceanogr. Res. Pap.,
759 39(9):1535-1552, doi: 10.1016/0198-0149(92)90046-V, 1992.

760 Harvey, W. A., and Caperon, J.: The rate of utilization of urea, ammonium, and nitrate
761 by natural populations of marine phytoplankton in a eutrophic environment, Pacific
762 Science, 30 (4), 329-340, http://hdl.handle.net/10125/1169, 1976.

763 Holmes, R., McClelland, J., Sigman, D., Fry, B., and Peterson, B.: Measuring $^{15}N–$
764 NH_4^+ in marine, estuarine and fresh waters: An adaptation of the ammonia diffusion
765 method for samples with low ammonium concentrations, Mar. Chem., 60, 235-243, doi:
766 10.1016/S0304-4203(97)00099-6, 1998.

767 Horrigan, S., Carlucci, A., and Williams, P.: Light inhibition of nitrification in
768 sea-surface films [California], J. Mar. Res., 1981.

769 Howard, M. D. A., Cochlan, W. P., Ladizinsky, N., and Kudela, R. M.: Nitrogenous
770 preference of toxigenic Pseudo-nitzschia australis (Bacillariophyceae) from field and
771 laboratory experiments, Harmful Algae, 6, 206-217, doi: 10.1016/j.hal.2006.06.003,
772 2007.

773 Hsiao, S.-Y., Hsu, T.-C., Liu, J.-w., Xie, X., Zhang, Y., Lin, J., Wang, H., Yang, J.-Y.,
774 Hsu, S.-C., and Dai, M.: Nitrification and its oxygen consumption along the turbid

775 Chang Jiang River plume, Biogeosciences, 11, 2083-2098, doi:
776 10.5194/bg-11-2083-2014, 2014.

777 Knapp, A. N., Sigman, D. M., and Lipschultz, F.: N isotopic composition of dissolved
778 organic nitrogen and nitrate at the Bermuda Atlantic Time-series Study site, Global
779 Biogeochem. Cycles, 19, doi: 10.1029/2004GB002320, 2005.

780 Koroleff, F.: Simultaneous oxidation of nitrogen and phosphorus compounds by
781 persulfate, Methods of seawater analysis, 2, 205-206, 1983.

782 Laws, E, A., and Wong, D. C. L.: Studies of carbon and nitrogen metabolism by three
783 marine phytoplankton species in nitrate−limited continuous culture, Journal of
784 Phycology, 14(4): 406-416, doi: 10.1111/j.1529-8817.1978.tb02460.x, 1978.

785 Laws, E. A.: Analytic Models of NH_4^+ Uptake and Regeneration Experiments, Limnol.
786 Oceanogr., 30, 1340–1350, doi: 10.4319/lo.1985.30.6.1340, 1985.

787 Laws, E. A., Landry, M. R., Barber, R, T., Lisa Campbellc, Mary-Lynn Dicksond, and
788 John Marra.: Carbon cycling in primary production bottle incubations: inferences from
789 grazing experiments and photosynthetic studies using ^{14}C and ^{18}O in the Arabian Sea,
790 Deep Sea Res. Part II Top. Stud. Oceanogr., 47(7): 1339-1352, doi:
791 10.1016/S0967-0645(99)00146-0, 2000.

792 Lipschultz, F.: A time-series assessment of the nitrogen cycle at BATS, Deep Sea Res.
793 Part II Top. Stud. Oceanogr., 48, 1897-1924, doi: 10.1016/S0967-0645(00)00168-5,
794 2001.

795 Lipschultz, F.: Isotope Tracer Methods for Studies of the Marine Nitrogen Cycle, in
796 Nitrogen in the marine environment, edited by: Capone, D. A., Bronk, D. A.,
797 Mulholland, M. R., Carpenter, E. J., Academic Press, London, U.K., 303-384, 2008.

798 Lomas, M. W., and Lipschultz, F.: Forming the primary nitrite maximum: Nitrifiers or
799 phytoplankton, Limnol. Oceanogr., 51, 2453-2467, doi: 10.4319/lo.2006.51.5.2453,
800 2006.

801 Luo, H., Tolar, B. B., Swan, B. K., Zhang, C. L., Stepanauskas, R., Ann, M. M., and
802 Hollibaugh, J. T.: Single-cell genomics shedding light on marine Thaumarchaeota
803 diversification, ISME Journal, 8, 732-736, doi: 10.1038/ismej.2013.202, 2014.

804 Marchant, H. K., Mohr, W., Kuypers, M. M. M.: Recent advances in marine N-cycle
805 studies using ^{15}N labeling methods. Curr. Opin. Biotechnol., 41, 53-59, doi:
806 10.1016/j.copbio.2016.04.019, 2016.

807 McCarthy, J. J., and Eppley, R. W.: A comparison of chemical, isotopic, and enzymatic
808 methods for measuring nitrogen assimilation of marine phytoplankton, Limnol.
809 Oceanogr., 17, 371-382, doi: 10.4319/lo.1972.17.3.0371, 1972.

Mccarthy, J. J., Taylor, and Taft, J. L.: Nitrogenous nutrition of the plankton in the Chesapeake Bay.1. Nutrient availability and phytoplankton preferences, Limnol. Oceanogr., 22, 996-1011, 1977.

McIlvin, M. R., and Altabet, M. A.: Chemical conversion of nitrate and nitrite to nitrous oxide for nitrogen and oxygen isotopic analysis in freshwater and seawater, Anal. Chem., 77, 5589-5595, doi: 10.1021/ac050528s, 2005.

Merbt, S. N., Stahl, D. A., Casamayor, E. O., Mart í E., Nicol, G. W., and Prosser, J. I.: Differential photoinhibition of bacterial and archaeal ammonia oxidation, FEMS Microbiol. Lett., 327, 41-46, doi: http://dx.doi.org/10.1111/j.1574-6968.2011.02457.x, 2012.

Middelburg, J. J., and Nieuwenhuize, J.: Uptake of dissolved inorganic nitrogen in turbid, tidal estuaries, Mar. Ecol. Prog. Ser., 192, 79-88, doi: 10.3354/meps192079, 2000.

Mulholland, M. R., and Lomas, M. W.: Nitrogen uptake and assimilation, in Nitrogen in the marine environment, edited by: Capone, D. A., Bronk, D. A., Mulholland, M. R., Carpenter, E. J., Academic Press, London, U.K., 303-384, 2008.

Newell, S. E., Fawcett, S. E., and Ward, B. B.: Depth distribution of ammonia oxidation rates and ammonia-oxidizer community composition in the Sargasso Sea, Limnol. Oceanogr., 58, 1491-1500, doi: 10.4319/lo.2013.58.4.1491, 2013.

Olson, R.: ^{15}N tracer studies of the primary nitrite maximum, J. Mar. Res., 39, 203-226, 1981a.

Olson, R. J.: Differential photoinhibition of marine nitrifying bacteria: a possible mechanism for the formation of the primary nitrite maximum, J. Mar. Res., 39, 227-238, 1981b.

Painter, S. C., Patey, M. D., Tarran, G. A., and Torres-Vald és, S.: Picoeukaryote distribution in relation to nitrate uptake in the oceanic nitracline, Aquat. Microb. Ecol., 72, 195-213, doi: 10.3354/ame01695, 2014.

Pakulski, J., Benner, R., Amon, R., Eadie, B., and Whitledge, T.: Community metabolism and nutrient cycling in the Mississippi River plume: evidence for intense nitrification at intermediate salinities, Mar. Ecol. Prog. Ser., 117, 207, 1995.

Peng, X., Fuchsman, C. A., Jayakumar, A., Warner, M. J., Devol, A. H., and Ward, B. B.: Revisiting nitrification in the eastern tropical South Pacific: A focus on controls, J. Geophys. Res.: Oceans, doi: 10.1002/2015JC011455, 2016.

Pfister, C. A., Altabet, M. A., Pather, S., and Dwyer, G.: Tracer experiment and model evidence for macrofaunal shaping of microbial nitrogen functions along rocky shores, Biogeosciences, 13, 3519-3531, doi: 10.5194/bg-13-3519-2016, 2016.

Raimbault, P., and Garcia, N.: Evidence for efficient regenerated production and dinitrogen fixation in nitrogen-deficient waters of the South Pacific Ocean: impact on new and export production estimates, Biogeosciences, 5, 323-338, 2008.

Santoro, A., Sakamoto, C., Smith, J., Plant, J., Gehman, A., Worden, A., Johnson, K., Francis, C., and Casciotti, K.: Measurements of nitrite production in and around the primary nitrite maximum in the central California Current, Biogeosciences, 10, 7395-7410, doi: 10.5194/bg-10-7395-2013, 2013.

Santoro, A. E., Casciotti, K. L., and Francis, C. A.: Activity, abundance and diversity of nitrifying archaea and bacteria in the central California Current, Environ. Microbiol., 12, 1989-2006, doi. L., and Francis, C. A.: Activity, abundance and diversity of nitrifying archaea and bacteria in the central California Current, Environ. Microbiol., 12, 1989-2006, 2010.

Santoro, A. E., Dupont, C. L., Richter, R. A., Craig, M. T., Carini, P., Mcilvin, M. R., Yang, Y., Orsi, W. D., Moran, D. M., and Saito, M. A.: Genomic and proteomic characterization of "Candidatus Nitrosopelagicus brevis": An ammonia-oxidizing archaeon from the open ocean, Proceedings of the National Academy of Sciences of the United States of America, 112, 1173-1178, doi: 10.1073/pnas.1416223112, 2015.

Sigman, D., Casciotti, K., Andreani, M., Barford, C., Galanter, M., and Böhlke, J.: A bacterial method for the nitrogen isotopic analysis of nitrate in seawater and freshwater, Anal. Chem., 73, 4145-4153, doi: 10.1021/ac010088e, 2001.

Smith, J. M., Chavez, F. P., and Francis, C. A.: Ammonium uptake by phytoplankton regulates nitrification in the sunlit ocean, PloS One, 9, e108173, doi: org/10.1371/journal.pone.0108173, 2014.

Sunda, W. G., and Ransom, H. D.: Ammonium uptake and growth limitation in marine phytoplankton, Limnol. Oceanogr., 52, 2496–2506, 2007.

van Kessel, M. A., Speth, D. R., Albertsen, M., Nielsen, P. H., Opden Camp, H. J., Kartal, B., Jetten, M. S., and Lucker, S.: Complete nitrification by a single microorganism, Nature, 528, 555-559, 10.1038/nature16459, doi: 10.1038/nature16459, 2015.

Varela, M. M., Bode, A., Fernandez, E., Gonzalez, N., Kitidis, V., Varela, M., and Woodward, E.: Nitrogen uptake and dissolved organic nitrogen release in planktonic communities characterised by phytoplankton size–structure in the Central Atlantic Ocean, Deep Sea Res. Part I Oceanogr. Res. Pap., 52, 1637-1661, doi: 10.1016/j.dsr.2005.03.005, 2005.

Veuger, B., Middelburg, J. J., Boschker, H. T. S., Nieuwenhuize, J., Rijswijk, P. V., Rochelle-Newall, E. J., and Navarro, N.: Microbial uptake of dissolved organic and

882 inorganic nitrogen in Randers Fjord, Estuarine Coastal and Shelf Science, 61, 507–515,
883 doi: 10.1016/j.ecss.2004.06.014, 2004.

884 Wada, E., and Hatton, A.: Nitrite metabolism in the euphotic layer of the central North
885 Pacific Ocean, Limnol. Oceanogr., 16, 766-772, doi: 10.4319/lo.1971.16.5.0766 1971.

886 Ward, B. B.: Temporal variability in nitrification rates and related biogeochemical
887 factors in Monterey Bay, California, USA, Mar. Ecol. Prog. Ser., 292, 109, doi:
888 10.3354/meps292097, 2005.

889 Ward, B. B.: Nitrification in marine systems, in Nitrogen in the marine environment,
890 edited by: Capone, D. A., Bronk, D. A., Mulholland, M. R., Carpenter, E. J., Academic
891 Press, London, U.K., 5, 199-261, 2008.

892 Ward, B. B.: Measurement and distribution of nitrification rates in the oceans, in
893 Methods in enzymology, edited by Abelson, J. N., Simon, M. I., Academic Press,
894 London, U.K., 486, 307-323, 2011.

895 Yool, A., Martin, A. P., Fernández, C., and Clark, D. R.: The significance of
896 nitrification for oceanic new production, Nature, 447, 999-1002, doi:
897 10.1038/nature05885, 2007.

898 Zehr, J. P., and Kudela, R. M.: Nitrogen cycle of the open ocean: from genes to
899 ecosystems, Ann. Rev. Mar. Sci., 3, 197-225, doi:
900 10.1146/annurev-marine-120709-142819, 2011.

901 Zhang, L., Altabet, M. A., Wu, T., and Hadas, O.: Sensitive measurement of NH_4^+
902 $^{15}N/^{14}N$ ($\delta^{15}NH_4^+$) at natural abundance levels in fresh and saltwaters, Anal. Chem., 79,
903 5297-5303, doi: 10.1021/ac070106d, 2007.

904 Zhu, Y., Yuan, D., Huang, Y., Ma, J., and Feng, S.: A sensitive flow-batch system for
905 on board determination of ultra-trace ammonium in seawater: Method development and
906 shipboard application, Anal. Chim. Acta., 794, 47-54, 10.1016/j.aca.2013.08.009, doi:
907 10.1016/j.aca.2013.08.009, 2013.

908

Table 1. The isotope matrix results for (A) the specific rates and (B) average rates of N processes in the low-nutrient case during the first interval under different r_{NH4+} variation conditions. And all N transformation rates via ODE following Pfister et al. (2016) on the assumption of no remineralization were estimated for comparison. Note r_{NH4+} variation was manipulated artificially by decreasing r_{NH4+} values at a constant reduction rate and the total reduction of r_{NH4+} was 0%, 1%, 10%, 20% and 50% of the full time span (24 h) of incubation.

(A)

Rate constant (k) h^{-1}	The percentage of r_{NH4+} decrease in 24 h					
	0		1%	10%	20%	50%
	ODE	Isotope Matrix				
NH_4^+ uptake (k1)	0.040	0.038	0.038	0.038	0.038	0.039
Remineralization (k2)	0	0	0.00001	0.0001	0.0002	0.001
NH_4^+ oxidation (k3)	0.0004	0.0005	0.0005	0.0005	0.0005	0.0005
NO_x^- uptake (k4)	0.060	0.059	0.059	0.059	0.059	0.059
DON release (k5)	0.017	0.024	0.024	0.024	0.024	0.024
Bacteria uptake NH_4^+ (k6)	0.005	0.007	0.008	0.011	0.015	0.028

(B)

Rate ($k \times \bar{C}$) nmol L^{-1} h^{-1}	The percentage of r_{NH4+} decrease in 24 h					
	0		1%	10%	20%	50%
	ODE	Isotope Matrix				
NH_4^+ uptake (F1)	3.8	4.9	4.9	4.9	5.0	5.1
Remineralization (F2)	0.0	0.0	0.1	0.6	1.2	3.0
NH_4^+ oxidation (F3)	0.04	0.07	0.1	0.1	0.1	0.7
NO_x^- uptake (F4)	19.3	27.2	27.2	27.2	27.2	27.2
DON release (F5)	9.6	11.5	11.5	11.6	11.6	11.8
Bacteria uptake NH_4^+ (F6)	0.5	1.0	1.0	1.5	2.0	3.7

Table 2. The isotope matrix results for the rates of N processes in the high-nutrient case at the depth of (A) 80% sPAR and (B) 2% sPAR under different r_{NH4+} variation conditions. And all N transformation rates via ODE following Pfister et al. (2016) on the assumption of no remineralization were estimated for comparison. Note: r_{NH4+} variation was manipulated artificially by decreasing r_{NH4+} values at a constant reduction rate and the total reduction of r_{NH4+} was 0%, 1%, 10%, 20% and 50% of the full time span (15 h) of incubation.

(A)

Rate ($k^* \bar{C}$) nmol L^{-1} h^{-1}	The percentage of r_{NH4+} decrease in 15 h					
	0		1%	10%	20%	50%
	ODE	Isotope Matrix				
NH_4^+ uptake (F1)	360	397	397	399	401	408
Remineralization (F2)	0	0	21	211	424	1043
NO_2^- uptake (F3)	27	29	29	29	29	29
NH_4^+ oxidation (F4)	1.1	0.4	0.4	0.4	0.4	0.4
NO_3^- uptake (F5)	190	149	149	149	149	149
NO_2^- oxidation (F6)	1.7	0	0	0	0	0
DON release (F7)	0	0	0	0	0	0
Bacteria uptake NH_4^+ (F8)	268	282	303	490	701	1314

(B)

Rate ($k^* \bar{C}$) nmol L^{-1} h^{-1}	The percentage of r_{NH4+} decrease in 15 h					
	0		1%	10%	20%	50%
	ODE	Isotope Matrix				
NH_4^+ uptake (F1)	228	208	208	209	211	216
Remineralization (F2)	0	0	18.1	179	361	895
NO_2^- uptake (F3)	7.3	3.1	3.1	3.1	3.1	3.1
NH_4^+ oxidation (F4)	1.1	0.7	0.7	0.7	0.7	0.7
NO_3^- uptake (F5)	106	72	72	72	72	72
NO_2^- oxidation (F6)	2.0	0	0	0	0	0
DON release (F7)	0	0	0	0	0	0
Bacteria uptake NH_4^+ (F8)	202	265	283	442	623	1152

927 **Table 3.** Comparison of the NH_4^+/ NO_x^- uptake and NH_4^+ oxidation/nitrification rates
928 derived from different methods.

Process	Case	Depth (m)	Isotope Matrix method (this study)	Rates based on Ref A*	Traditional method Ref B*	Rates followed Ref C*
			(nmol L^{-1} h^{-1})			
NH_4^+ uptake	Low nutrient	25	4.9	3.8	4.6	
Nitrification	Low nutrient	25	0.07	0.04	−	0.05
NO_x^- uptake	Low nutrient	25	27.2	19.3		4.6
NH_4^+ uptake	High -80%sPAR	0.2	397	360	387	
NH_4^+ oxidation	High -80%sPAR	0.2	0.4	1	−	
NH_4^+ uptake	High -2% sPAR	2.3	208	228	192	
NH_4^+ oxidation	High -2% sPAR	2.3	0.7	1	−	

929 Ref A* stands of rates calculation by ODE followed Pfister et al. (2016)

930 Ref B* stands of rates calculation followed Collos (1987)

931 Ref C* stands of rates calculation followed Santoro et al. (2010)

932

Table 4. The contribution of nitrification derived NO_x^- to NO_x^- uptake (%), N preference index, and the proportion of NH_4^+ consumption by phytoplankton, bacteria and nitrifier to total NH_4^+ consumption in low and high nutrient cases.

Case	Depth (m)	nitrification to NO_3^- uptake (%)	RPI for NH_4^+	RPI for NO_2^-	RPI for NO_3^-	*A/TNH_4^+ consumption (%)	*B/TNH_4^+ consumption (%)	*C/TNH_4^+ consumption (%)
Low nutrient	25	0.3	0.9		1.0	82.1	16.8	1.2
High -80%sPAR	0.2	0.3	1.6	0.6	0.5	58.4	41.5	0.1
High -2% sPAR	2.3	0.9	1.8	0.1	0.5	43.9	56.0	0.1

*A, *B, *C stands for NH_4^+ utilized by phytoplankton, bacteria and nitrifier, respectively. TNH_4^+ consumption stands for total NH_4^+ consumption.

939 **Figure Captions**

940 **Fig. 1.** Model schemes with the most fundamental nitrogen transformation processes in
941 low- (a) and high- (b) nutrient aquatic environments. Arrows stand for the transfer
942 flux/rate from the reactant to product pool. The structure and inter-exchanges in the
943 high-nutrient case (Fig. 1b) are the same as in (a), except that NO_x^- is divided into NO_2^-
944 and NO_3^-.

945 **Fig. 2.** The observational data in the low-nutrient case for (a) $[NH_4^+]$, (b) $[NO_x^-]$, (c)
946 [PN], (d) [TDN], (e) $\delta^{15}N\text{-}NO_x^-$, (f) $\delta^{15}N$-PN. The regular and inverse open triangles
947 stand for the paralled samples and the analytical errors are shown.

948 **Fig. 3.** The observational data in the high-nutrient case for (a) $[NH_4^+]$, (b) $[NO_2^-]$, (c)
949 $[NO_3^-]$, (d) [PN], (e) [TDN], (f) [PN+TDN], (g) $\delta^{15}N\text{-}NO_2^-$, (h) $\delta^{15}N\text{-}NO_3^-$ and (i)
950 $\delta^{15}N$-PN. The light and dark red diamonds stand for the paralled samples in 80%
951 sPAR case and the black regular and inverse open triangles stand for the paralled
952 samples in 2% sPAR case. The analytical errors are shown in figures.

953 **Fig. 4.** The observed and STELLA-derived values in the low-nutrient case for (a)
954 $[^{15}NH_4^+]$, (b) $[^{15}NO_x^-]$, (c) [^{15}N-PN], (d) [^{15}N-DON], (e) $[^{14}NH_4^+]$, (f) $[^{14}NO_x^-]$, (g)
955 [^{14}N-PN], (h) [^{14}N-DON], (i) r_{NH4+}, (j) r_{NOx-}, (k) r_{PN}, (l) r_{DON}, (m) $\delta^{15}N\text{-}NH_4^+$, (n)
956 $\delta^{15}N\text{-}NO_x^-$, (o) $\delta^{15}N$-PN, (p) $\delta^{15}N$-DON, (q) $[NH_4^+]$, (r) $[NO_x^-]$, (s) [PN] and (t)
957 [DON]. The black regular and inverse open triangles represent the paralleled observed
958 values; the black, green, blue, magenta and pink solid lines stand for the STELLA
959 model simulations when r_{NH4+} decreases 0%, 1%, 10%, 20% and 50% in 24 h,
960 respectively. The dashed lines in (b), (f), (j), (n) and (r) were generated from nonlinear
961 least-squares curve-fitting by Matlab following Santoro et al. (2010).

962 **Fig. 5.** The observed and STELLA-derived values in the high-nutrient case of (A) 80%
963 sPAR depth and (B) 2% sPAR depth for (a) $[^{15}NH_4^+]$, (b) $[^{15}NO_2^-]$, (c) $[^{15}NO_3^-]$, (d)
964 [^{15}N-PN], (e) [^{15}N-DON], (f) $[^{14}NH_4^+]$, (g) $[^{14}NO_2^-]$, (h) $[^{14}NO_3^-]$, (i) [^{14}N-PN], (j)

965 [^{14}N-DON], (k) r_{NH4+}, (l) r_{NO2-}, (m) r_{NO3-}, (n) r_{PN}, (o) r_{DON}, (p) δ^{15}N-NH_4^+, (q)
966 δ^{15}N-NO_2^-, (r) δ^{15}N-NO_3^-, (s) δ^{15}N-PN, (t) δ^{15}N-DON, (u) [NH_4^+], (v) [NO_2^-], (w)
967 [NO_3^-] (x) [PN] and (y) [DON]. The black regular and inverse open triangles
968 represent the duplicate observational values; the black, green, blue, magenta and pink
969 solid lines represent the STELLA model simulations of r_{NH4+} decreases 0%, 1%, 10%,
970 20% and 50% in 15 h, respectively.
971

972 **Fig. 1**

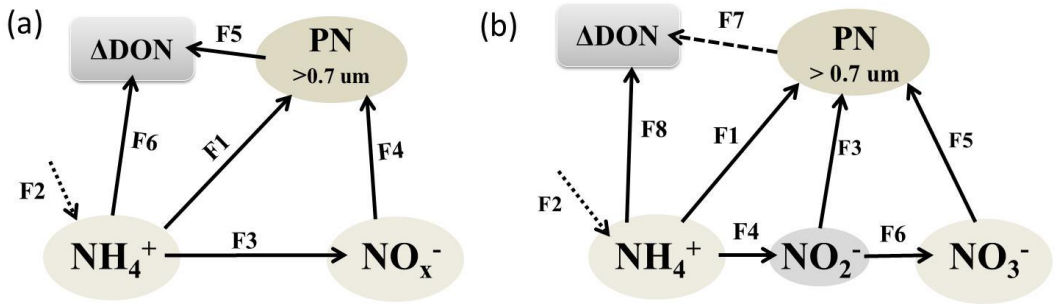

973

974

975 **Fig. 2**

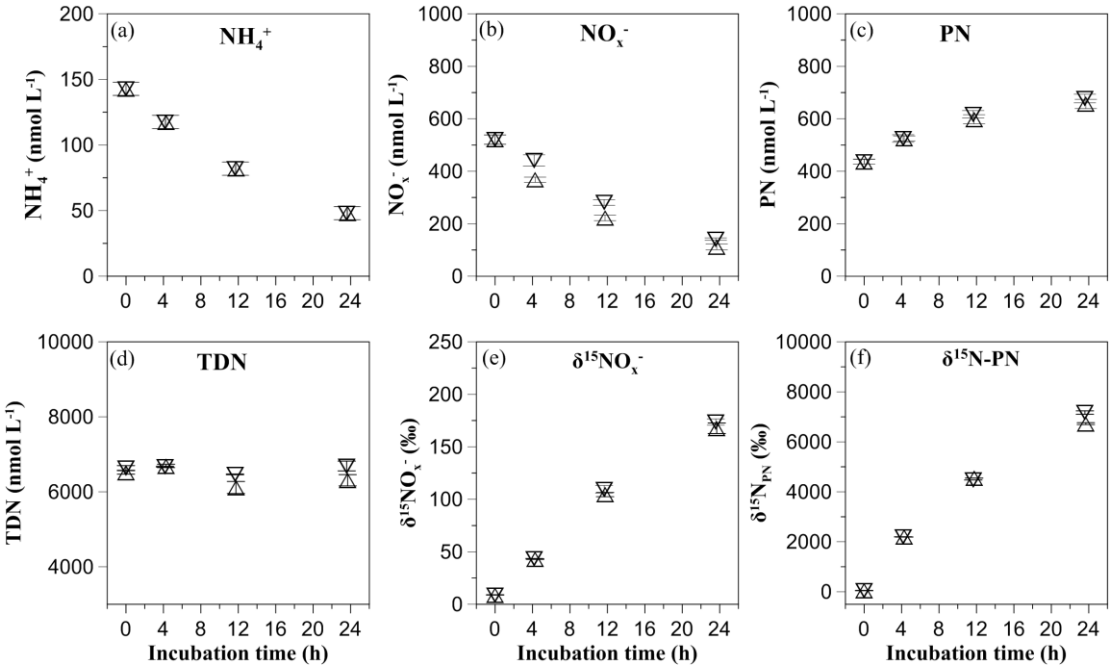

976

977

978 **Fig. 3**

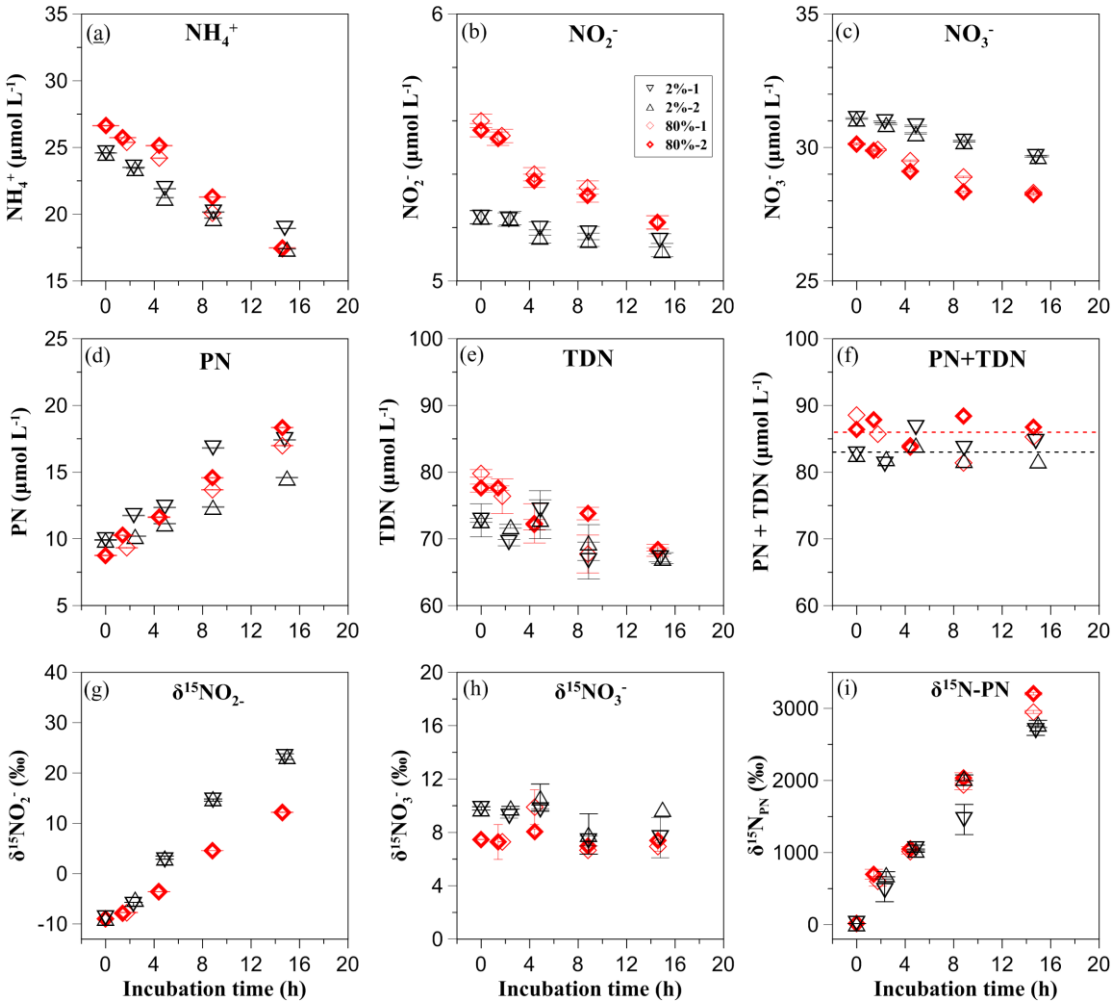

979

980

Fig. 4

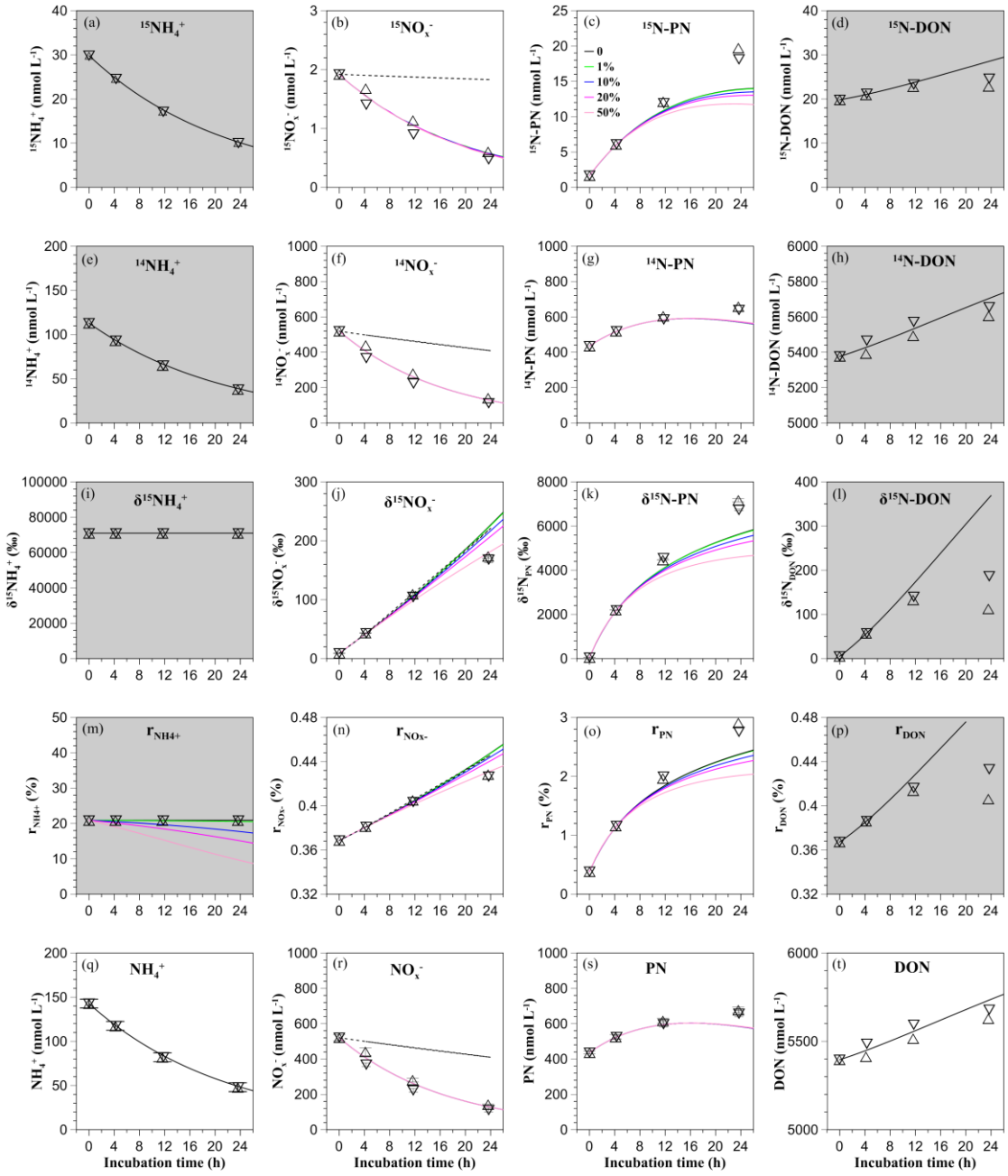
(a) $^{15}NH_4^+$
(b) $^{15}NO_x^-$
(c) ^{15}N-PN
(d) ^{15}N-DON
(e) $^{14}NH_4^+$
(f) $^{14}NO_x^-$
(g) ^{14}N-PN
(h) ^{14}N-DON
(i) $\delta^{15}NH_4^+$
(j) $\delta^{15}NO_x^-$
(k) δ^{15}N-PN
(l) δ^{15}N-DON
(m) r_{NH4+}
(n) r_{NOx-}
(o) r_{PN}
(p) r_{DON}
(q) NH_4^+
(r) NO_x^-
(s) PN
(t) DON
0
1%
10%
20%
50%
Incubation time (h)

Fig. 5(A)

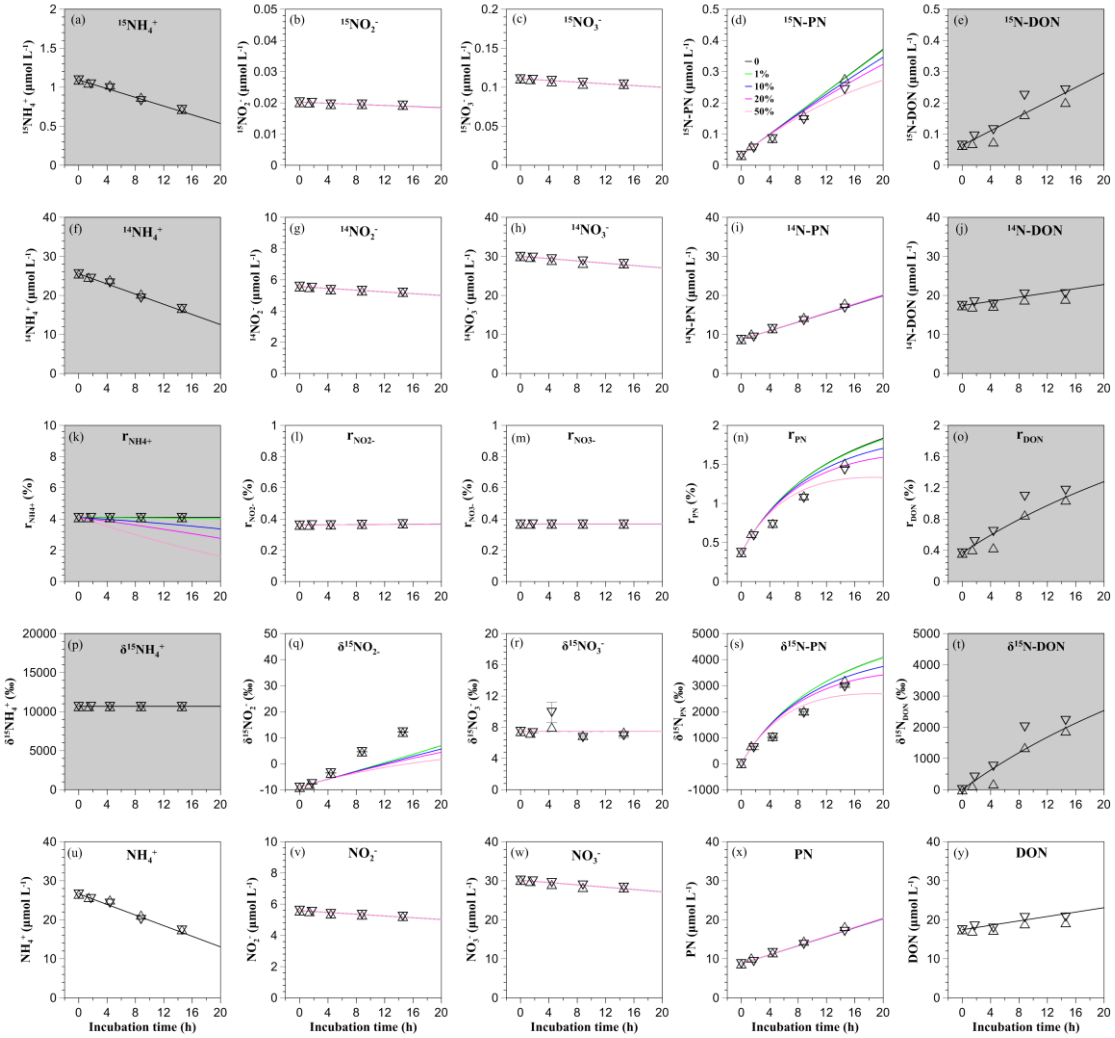
(a) $^{15}NH_4^+$
(b) $^{15}NO_2^-$
(c) $^{15}NO_3^-$
(d) ^{15}N-PN
0
1%
10%
20%
50%
(e) ^{15}N-DON
(f) $^{14}NH_4^+$
(g) $^{14}NO_2^-$
(h) $^{14}NO_3^-$
(i) ^{14}N-PN
(j) ^{14}N-DON
(k) r_{NH4+}
(l) r_{NO2-}
(m) r_{NO3-}
(n) r_{PN}
(o) r_{DON}
(p) $\delta^{15}NH_4^+$
(q) $\delta^{15}NO_2^-$
(r) $\delta^{15}NO_3^-$
(s) $\delta^{15}N$-PN
(t) $\delta^{15}N$-DON
(u) NH_4^+
(v) NO_2^-
(w) NO_3^-
(x) PN
(y) DON
Incubation time (h)

Fig. 5(B)

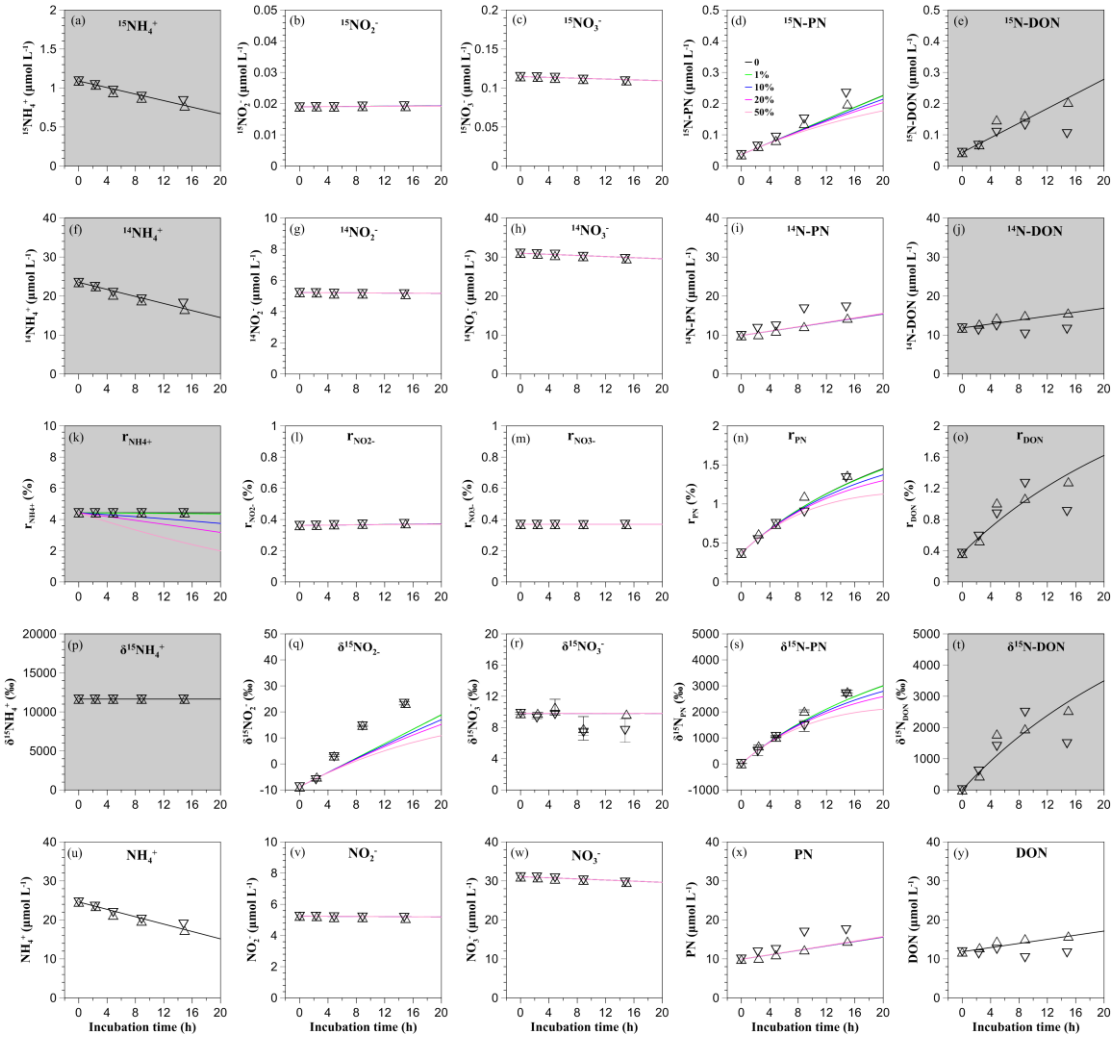
(a) $^{15}NH_4^+$
(b) $^{15}NO_2^-$
(c) $^{15}NO_3^-$
(d) ^{15}N-PN
(e) ^{15}N-DON
(f) $^{14}NH_4^+$
(g) $^{14}NO_2^-$
(h) $^{14}NO_3^-$
(i) ^{14}N-PN
(j) ^{14}N-DON
(k) r_{NH4+}
(l) r_{NO2-}
(m) r_{NO3-}
(n) r_{PN}
(o) r_{DON}
(p) $\delta^{15}NH_4^+$
(q) $\delta^{15}NO_2^-$
(r) $\delta^{15}NO_3^-$
(s) δ^{15}N-PN
(t) δ^{15}N-DON
(u) NH_4^+
(v) NO_2^-
(w) NO_3^-
(x) PN
(y) DON
0
1%
10%
20%
50%
Incubation time (h)